TAMPEREEN TEKNILLINEN YLIOPISTO
TAMPERE UNIVERSITY OF TECHNOLOGY

AIDIN ALINEZHAD KORDMAHALEH

ELECTRIFICATION OF HYDRAULIC SYSTEM

Master of Science Thesis

Examiner: prof. Seppo Tikkanen
Examiner and topic approved by the Faculty Council of the Faculty of Engineering sciences on 1st November 2017

ABSTRACT

AIDIN ALINEZHADKORDMAHALEH: Electrification of hydraulic system
Tampere University of technology
Master of Science Thesis, 47 pages, 6 Appendix pages
March 2018
Master's Degree Programme in Automation Engineering
Major: Fluid Power
Examiner: Professor Seppo Tikkanen

Keywords: Electrification of hydraulic system, PMSM, electric circuit, hydraulic circuit.

The master thesis consists of modeling one mobile hydraulic machine, ***Ponsse CARIBOU S10***, in both hydromechanical and electrohydraulic versions. In hydromechanical section, the drive line will be simulated. During simulation process, the performance and operation of hydraulic systems and its fuel consumption in the various conditions will be analyzed. Then, the diesel engine of the hydromechanical system will be replaced with battery driven Permanent Magnet Synchronous Motor (PMSM) in the simulation process, and the new model performance will be compared with the previous one.

PREFACE

This master has been done in the Laboratory of Automation and Hydraulic (AUT) at the Tampere University of Technology (TUT) during the years 2017-2018.

I donate this master thesis to my family which had open hug for my crying all the time. I never forget my father help for supporting me financially to continue the education abroad.

March 7th,2017

Language Center, Tampere University of Technology

Aidin Alinezhad Kordmahaleh

CONTENTS

LIST OF FIGURES

LIST OF SYMBOLS AND ABBREVIATIONS

Mechanical Parameters:

B	Bulk module
I_m	Inertia of hydraulic system
R_{GR}	Conversion ratio (Gear ratio)
R_p	Conversion ratio of pump
R_m	Conversion ratio of motor
$V_{max,l}$	Maximum velocity of loader
$T_{max,l}$	Maximum torque of hydraulic system
P_{diesel}	Diesel engine power
P_{boost}	Boost pump power
V_{gp}	Volumetric displacement of pump
V_{gm}	Volumetric displacement of motor
V_{hose}	Volume of hose
Q_p	Volumetric flow of pump
Q_m	Volumetric flow of motor
F	Traction force
V	Velocity
T_m	Torque of motor
T_p	Torque of pump
$T_{friction}$	Torque of friction
i_G	Gear ratio
n_{max}	Maximum rotational speed of motor
r_w	Radius of wheel
Δp_{in}	system pressure
η_{vp}	Volumetric efficiency of pump
η_{mp}	Mechanical efficiency of pump
η_{tp}	Total efficiency of pump
η_{vm}	Volumetric efficiency of motor
η_{mm}	Mechanical efficiency of motor
η_{tm}	Total efficiency of pump
η_g	Efficiency of gear ratio
ε_p	Relative volumetric displacement of pump
ε_m	Relative volumetric displacement of motor

Magnetic Parameters:

B	Viscous coefficient
I_e	PMSM inertia
R_s	Stator resistance
L_s	Stator inductance
L_{dq}	Inductance (d-q domain)
L_d	Inductance (direct axis)
L_q	Inductance (quadrature axis)

T_e	Electromagnetic torque
T_m	Load torque
i_{dq}	Current (d-q domain)
i_d	Current (direct axis)
i_q	Current (quadrature axis)
p	Number of poles
u_{dq}	Voltage (d-q domain)
u_d	Voltage (direct axis)
u_q	Voltage (quadrature axis)
f_s	Switching frequency of inverter
λ_{dq}	flux linkage
λ_{pm}	magnetic flux
ω_r	Angular velocity

1. INTRODUCTION

Nowadays, development of engineering systems needs modeling and simulation tools in where the new developing methods which includes complicated numerical process, can be implemented accurately. It leads to saving the time and cost of development. Undoubtedly, the computers can solve mathematical process fast and avoids producing a prototype for testing the new system [1].

The Mobile Hydraulic field is one of the best examples of using simulation tools for improving the system performance in where the significant dimensions of actuators, pumps, and motors as well as the high pressure of operation cause producing of the prototype to be unreasonable.

Recently, due to air pollution and fuel price issues around the world, the AC drives applications in vehicles are obtaining attention for example cranes. In the hybrid vehicles, the electrical system is based on AC motor winding configuration in where the torque is produced by the inverter [2].

1.1 Objective of the study

The objective of this research is modeling one mobile hydraulic machine, ***Ponsse CARIBOU S10***, in both hydromechanical and electrohydraulic versions. In hydromechanical view, the drive line will be simulated. During simulation process, the performance and operation of hydraulic systems and its fuel consumption in the various conditions will be analyzed. Then, the diesel engine of the hydromechanical system will be replaced with battery driven Permanent Magnet Synchronous Motor (PMSM) in the simulation process, and the new model performance will be compared with the previous one.

The main problem that will be evaluated in this master thesis is efficiency differences between hydromechanical system and PMSM system corresponding to the robustness and smooth behavior of parameters in these two systems. It should be checked that how the efficiency of PMSM system differ to the efficiency of current system.

In hydromechanical drive line case, the diesel engine will operate in variable rotational speed according to traction force and velocity. The hydraulic pump and motor efficiencies are not constant, and they vary along with rotational speed, displacement, and pressure. Therefore, the modeled mechanical efficiency can be close to the reality. Then, the PMSM system will be modeled with Field Oriented Control (FOC) method which is one the most precise controller in the PMSM technology. Apparently, the gained efficiency will be close to the reality again. In this way, the two systems can be compared.

1.2 Method of research

In this research, the MATLAB – Simulink has been used as the tool of modeling. Complicated chain calculation in real-time simulation can be done only by powerful analyzing software. Besides, the huge modeled machine with large dimensions and high parameters causes using prototype to be cost and time wasting. With Simulink, the system can be run several times by various inputs and all parameters can be measured without using any sensors or consuming power. It also reduces the possibility of errors in results due to avoiding handy calculation.

1.3 Outline of the thesis

This thesis report has four chapters: 1- Introduction 2- Theory of Drive Line and PMSM 3- Results 4- Discussion and conclusion

In chapter 2, the simulation model of driveline will be demonstrated in detail which includes control, hydraulic and load. All related hydraulic equations will be explained. Then, the theory of PMSM and the Field Oriented Method (FOM) are explained with mathematical equations and then, the Simulink model will be demonstrated in detail.

In chapter 3, the result of this simulation for both drive-line and PMSM model will be presented according to different reference inputs, and some ideas will be suggested for future development

In chapter 4, the main conclusions of simulations will be discussed and then, some tips about capability of the simulated model in wider perspective, its advantages and limitation will be explored.

2. THEORY OF DRIVE LINE AND PMSM

As it was mentioned, the modeled hydraulic driven machine is the Ponsse CARIBOU S10 (Figure 1). The drive line contains diesel engine, hydraulic pump, hydraulic motor and hose (Figure 2). The diesel engine drives the hydraulic pump then it transmits the hydraulic power to the hydraulic motor through hoses. Depended on the selected speed range, the gear box converts the rotational speed and torque of hydraulic motor to the necessary rotational speed and torque of wheel.

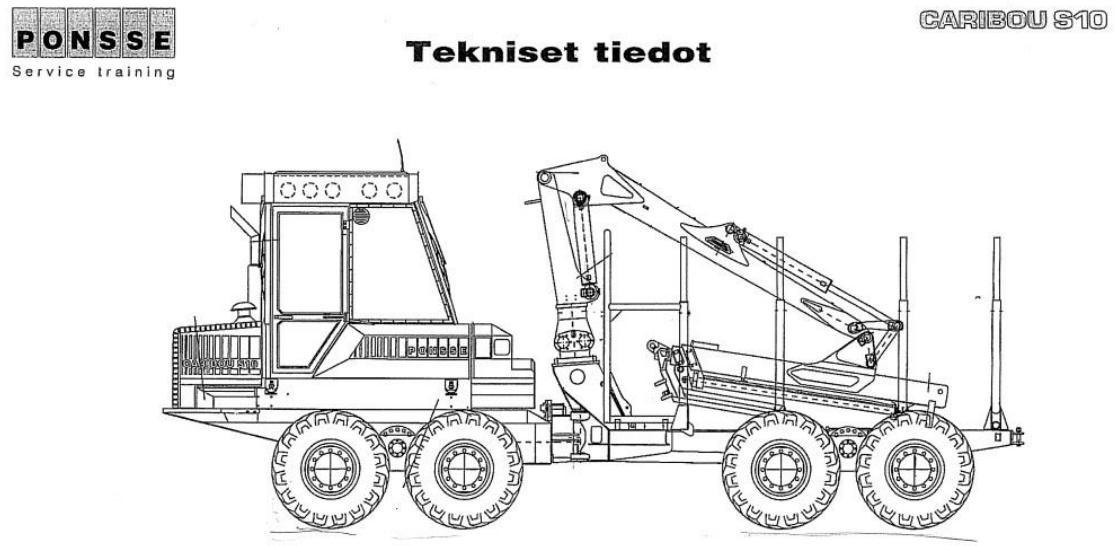

Figure 1. *Ponsse CARIBOU S10*

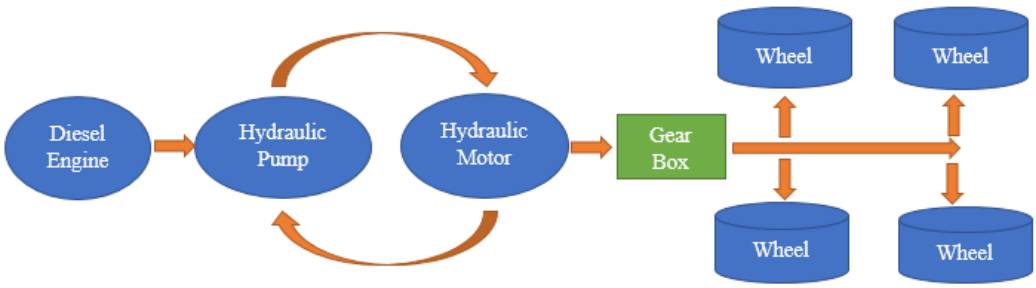

Figure 2. *Drive line schematic*

Table 1. *Ponsse CARIBOU S10 Parameters*

Main Parameters of Ponsse CARIBOU S10	
Maximum Power	91 kW
Maximum Traction Force	130 kN
Maximum Velocity	27 km/h
Weight	11950 kg

The simulation model includes reference block and drive line block (Figure 3). In Reference block, the reference velocity and traction force for loader are assigned, and then, they are implemented as the inputs in drive line block. At the end, the simulated speed and traction force will be compared with reference values. Figure 3 shows the general view of driveline simulation.

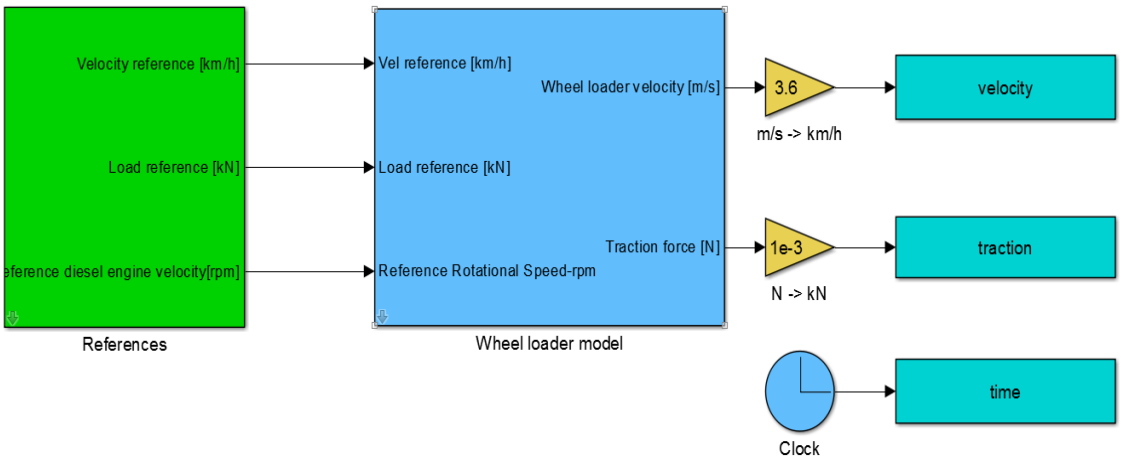

Figure 3. *The general view of driveline simulation*

In this chapter, firstly, the general model of drivelines with fundamental equations will be defined. Then, all blocks of Simulink will be introduced in detail, and finally, the range of traction force and gear ratio will be computed for two speed range, between 0 and 8 km/h and between 0 and 27 km/h. It should be mentioned that the diesel engine rotational

speed and pump/motor efficiencies are not constant and also the fuel consumption will be mapped based on proportional torque at nominal speed, relative rotational speed and relative power of diesel.

2.1 Drive Line theory in the hydraulic system

The first parameter that should be considered for modeling of a hydraulic system is Conversion Ratio which is the ratio of maximum power per available power.

$$R_{CR} = \frac{V_{max.l} * T_{max.l}}{(P_{diesel} - P_{boost}) * \eta_g * \eta_{tp} * \eta_{tm}} \quad (2-1)$$

In where, $V_{max.l}$ is maximum velocity of loader, $T_{max.l}$ is the maximum traction force, $\eta_g$is the efficiency of gear ratio, $\eta_{tp}$is the total efficiency of hydraulic pump, $\eta_{tm}$is the total efficiency of hydraulic motor, $P_{diesel}$is the diesel engine power and $P_{boost}$is boost pump power.

In the hydraulic system where the Conversion Ratio is usually bigger than three, therefore:

$$R_p = \sqrt{R_{CM}} \quad (2-2)$$

$$R_m = \sqrt{R_{CM}} \quad (2-3)$$

They are Conversion Ratio of pump and motor respectively. The maximum displacement of the hydraulic pump can be calculated by:

$$V_{gp} = \frac{V_{max.l} * T_{max.l}}{n_{diesel} * \Delta p_{in} * \eta_g * \eta_{tp} * \eta_{tm} * R_m} \quad (2-4)$$

In where, $n_{diesel}$is the rotational speed of diesel engine and $\Delta p_{in}$is the difference pressure in the both sides of the hydraulic pump.

Then with equations below, the maximum displacement of the hydraulic motor can be gained by:

$$n_{max.m} = \frac{V_{max.l} * i_G}{2 * \pi * r_w} \quad (2-5)$$

$$V_{gm} = \frac{V_{max.l} * T_{max.l}}{n_{diesel} * \Delta p_{in} * \eta_g * \eta_{mm}} \quad (2-6)$$

$$V_{gm} = \frac{2 * \pi * r_w * T_{max.l}}{\Delta p_{in} * i_G * \eta_{mm} * \eta_g} \quad (2-7)$$

Where i_G is the Gear Ratio, $r_w$is the loader wheel radius and η_{mm} is the mechanical efficiency of the hydraulic motor. It is not necessary to mention that the answers of equations (2-6) and (2-7) should be the same.

Now, the range of traction force and velocity should be determined by ***Corner Power Theory***. Figure 4 demonstrates the Corner Power definition in which by increasing the speed (point 1), the traction force will be decreased (point 2).

By mentioned theory, that the lowest speed at highest traction force and minimum traction force at maximum speed should be calculated:

$$Q_{p.1} = \left(\frac{P_{diesel} - P_{boost}}{\Delta p_{in}}\right) * \eta_{tp} \qquad (2-8)$$

$$V_{gp.1} = \frac{Q_{p1}}{n_{diesel} * \eta_{vp}} \qquad (2-9)$$

$$T_{m.1} = \frac{V_{gm} * \Delta p_{in} * \eta_{mm}}{2 * \pi} \qquad (2-10)$$

$$n_{m.1} = \frac{\left(Q_{p1} * \ \eta_{vm}\right)}{V_{gm}} \qquad (2-11)$$

$$F_1 = \frac{\left(T_{m.1} * i_G * \eta_g\right)}{r_w} \qquad (2-12)$$

$$V_1 = \frac{(2 * \pi * r_w * n_{m.1})}{i_G} \qquad (2-13)$$

In where, $Q_{p1}$is volumetric flow of the hydraulic pump in point 1, $V_{gp.1}$is the volumetric displacement of the hydraulic pump in point 1, $\eta_{vp}$is the volumetric efficiency of hydraulic pump, $T_{m.1}$is the torque of hydraulic motor in point 1, $n_{m.1}$ is the rotational speed of hydraulic motor in point 1, $\eta_{vm}$is the volumetric efficiency of hydraulic pump in point 1, $F_1$is the traction force (maximum) in point 1 and V_1 is the velocity of loader in point 1.

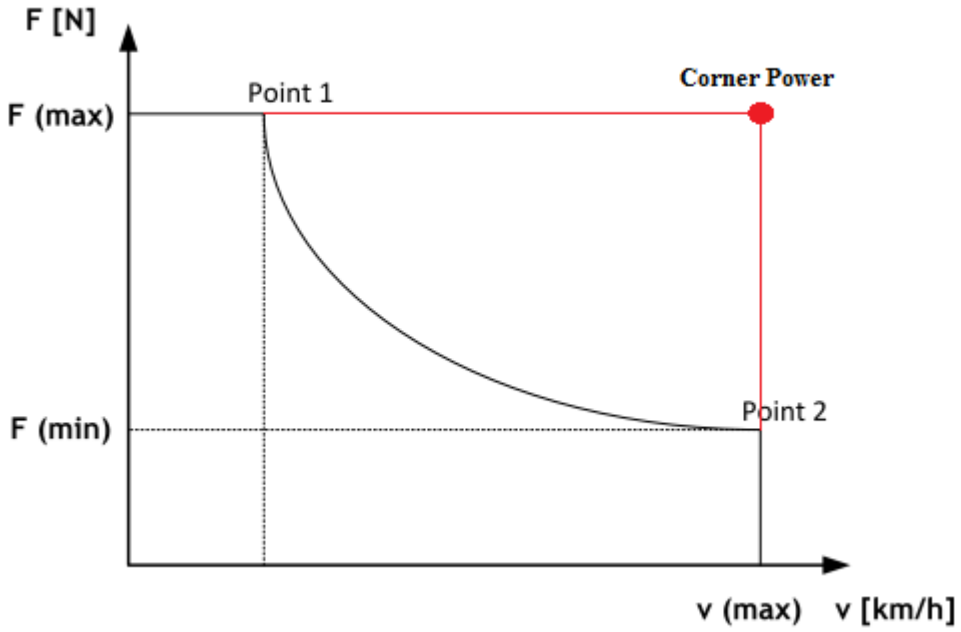

Figure 4. *The Corner Power Theory*

The lowest speed gains with the equation 13 (point 1). At point 2, the minimum traction force is computed by:

$$Q_{p.2} = \left(V_{gp} * n_{diesel} * \eta_{vp}\right) \quad (2-14)$$

$$\Delta p_2 = \left(\frac{(P_{diesel} - P_{boost}) * \eta_{tp}}{Q_{p.2}}\right) \quad (2-15)$$

$$V_{gm.2} = \frac{\left(Q_{p.2} * \eta_{vm}\right)}{n_{m.max}} \quad (2-16)$$

$$T_{m.2} = \frac{(V_{gm.2} * \Delta p_2 * \eta_{mm})}{2 * \pi} \quad (2-17)$$

$$F_2 = \frac{\left(T_{m.2} * i_G * \eta_g\right)}{r_w} \quad (2-18)$$

$$V_2 = \frac{(2 * \pi * r_w * n_{m.max})}{i_G} \quad (2-19)$$

In where, $Q_{p.2}$ is the volumetric flow of the hydraulic pump in point 2, Δp_2 is the pressure of the system in point 2, $V_{gm.2}$ is the volumetric displacement of hydraulic motor in point 2, $n_{m.max}$ is the maximum rotational speed of hydraulic motor (catalogue), $T_{m.2}$ is the

torque of the hydraulic pump at point 2, F_2 is the traction force in point 2 and V_2 is the velocity of loader in point 2.

2.2 Simulation model of drive line

In Figure 3, the outside view of drive line simulation has been presented. In this section, all simulation blocks will be explained in detailed.

2.2.1 References

Figure 5 shows the detail of reference block in where the trend of velocity and traction force during the simulation time have been implemented. All reference values have a transfer function due to the delay. The traction force reference runs with the first order delay and velocity and diesel engine rotational speed run with the second order delay. It is not necessary to repeat that the trends for velocity and traction force should be logical, based on Corner Power Theory.

2.2.2 Forwarder Model

As Figure 6 shows the modeled forwarder has four main sub-blocks: Diesel Engine, Pump and Motor controllers (displacement), Hydrostatics, and Load. Their collaboration in Simulink causes the drive application can be modeled. In next sections, these sub-blocks will be described comprehensively.

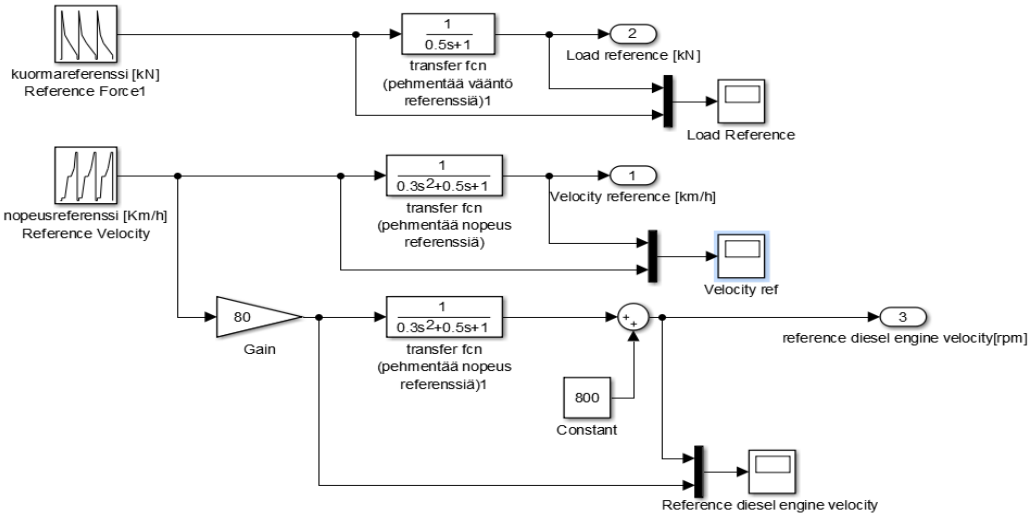

Figure 5. *Simulation model of reference block*

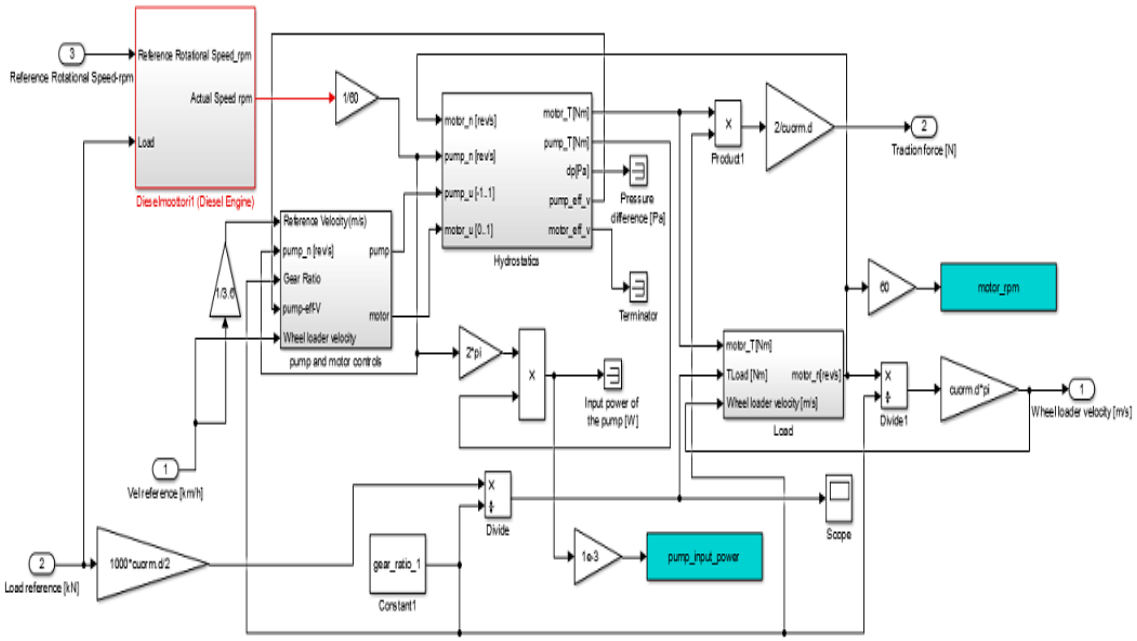

Figure 6. *Simulation model of forwarder*

Diesel Engine

The main point in Diesel engine simulation is that the rotational speed is not constant. There is an ideal rotational speed (800 rpm, implemented in reference block), and then it varies according to reference velocity and load torque that is induced by traction force. The effects of velocity and traction force on rotational speed is showed in Figure 7.

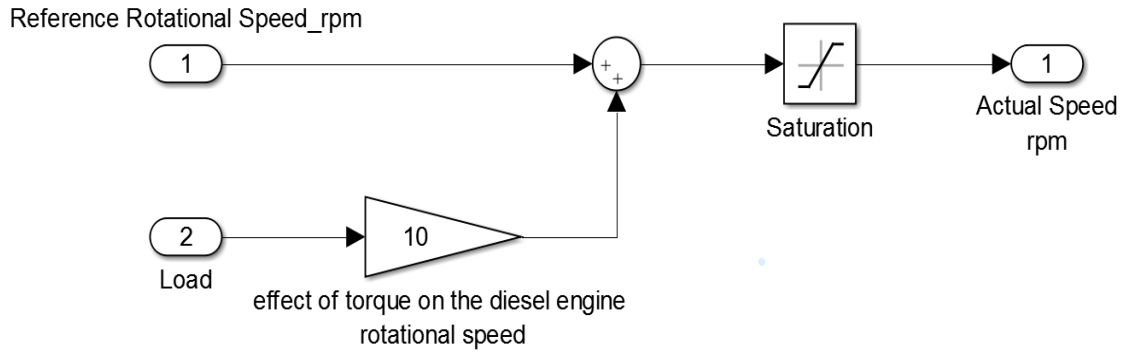

Figure 7. *Simulation model of diesel engine*

Pump and Motor Control

In hydraulic driveline theory, for raising the velocity, there are two separate functions: the rotational speed and volumetric displacement of the pump should increase firstly. In this period, the volumetric displacement of the motor is equal to 1 (range 0-1). After reaching the highest values, the second function should be active. In this step, the volumetric displacement of the pump is equal to 1, and the volumetric displacement of motor begins to reduce gradually. When the pump parameters achieve the maximum level, the flow rate in the circuit will be constant, therefore, by reducing the displacement of the motor, it is possible to increase the rotational speed of pump more.

In Figure 8, the reference velocity has some delay due to the gas pedal. Then it should change to the small scale (volumetric displacement range) according to the range of speed. Math function block leads to reducing the motor displacement when the pump displacement gains 1.

Hydrostatics

As it is shown in Figure 9, this block has three main sub-blocks: hydraulic pump, hydraulic motor, and hoses. The Hydraulic pump and motor have been modeled corresponding to their mathematical equations:

$$T_{p.boost} = \frac{\Delta p_p * V_{gp.boost}}{\eta_{mp.boost}} \qquad (2-20)$$

$$T_p = \frac{\varepsilon_p * V_{gp.pump} * \Delta p_p}{\eta_{mp.pump}} \qquad (2-21)$$

$$T_m = \varepsilon_{pm} * V_{gp.motor} * \Delta p_m * \eta_{mp.motor} \qquad (2-22)$$

$$Q_p = \varepsilon_p * V_{gp.pump} * n_p * \eta_{vp} \qquad (2-23)$$

$$Q_m = \frac{\varepsilon_m * V_{gp.motor} * n_m}{\eta_{vm}} \qquad (2-24)$$

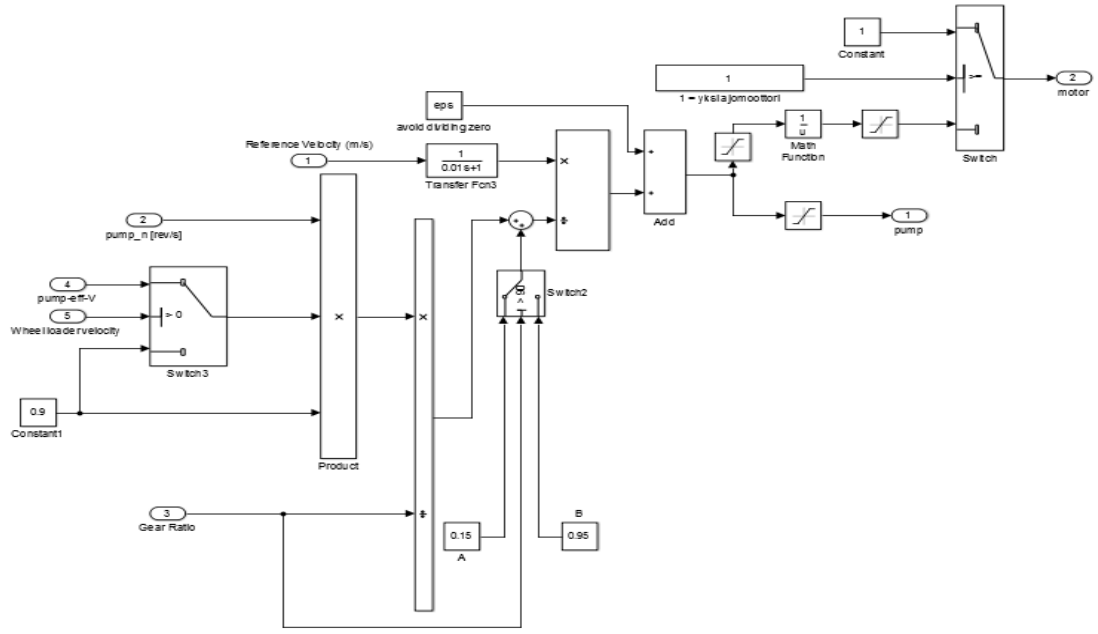

Figure 8. *Simulation model of controller*

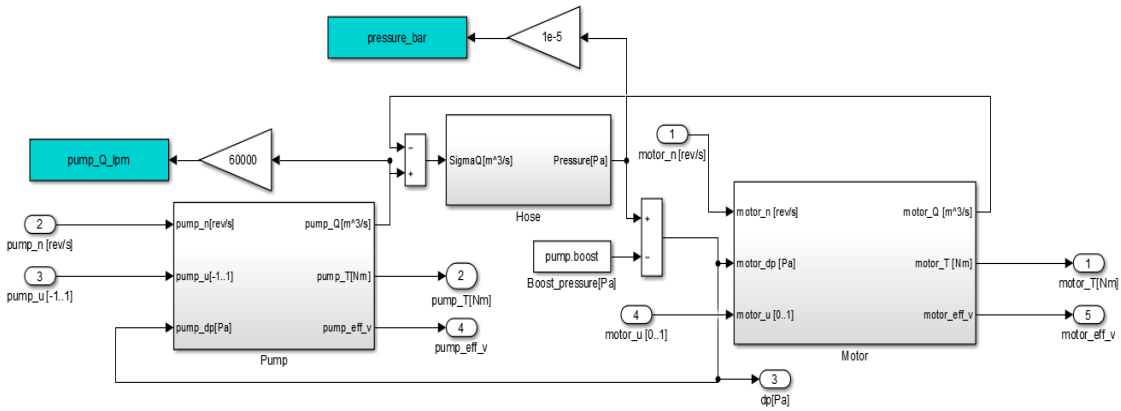

Figure 9. *Simulation model of the hydrostatic*

In the hose simulation, the state equation of volume has been implemented.

$$\frac{dp}{dt} = \frac{B * \Sigma Q}{V_{hose}} \qquad (2-25)$$

Where the B is the bulk module in the hose, V_{hose} is the volume of the hose and ΣQ is the net flow of hose volume (difference between the volume flow of hydraulic pump and hydraulic motor).

In Figures 10,11, and 12 are simulations of the hose, hydraulic pump and hydraulic motor respectively.

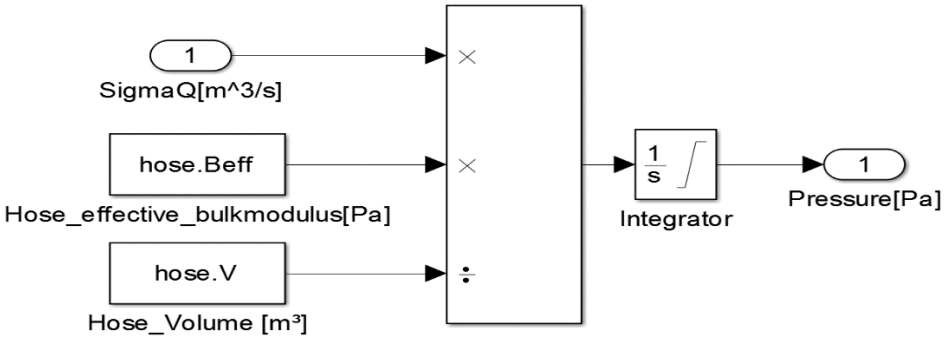

Figure 10. *Simulation model of the hose*

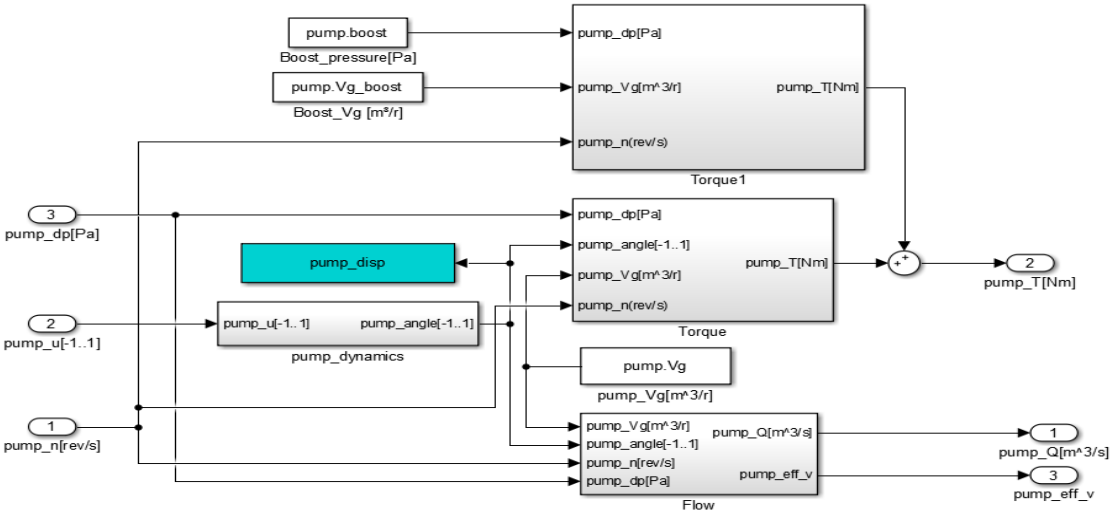

Figure 11. *Simulation model of the hydraulic pump*

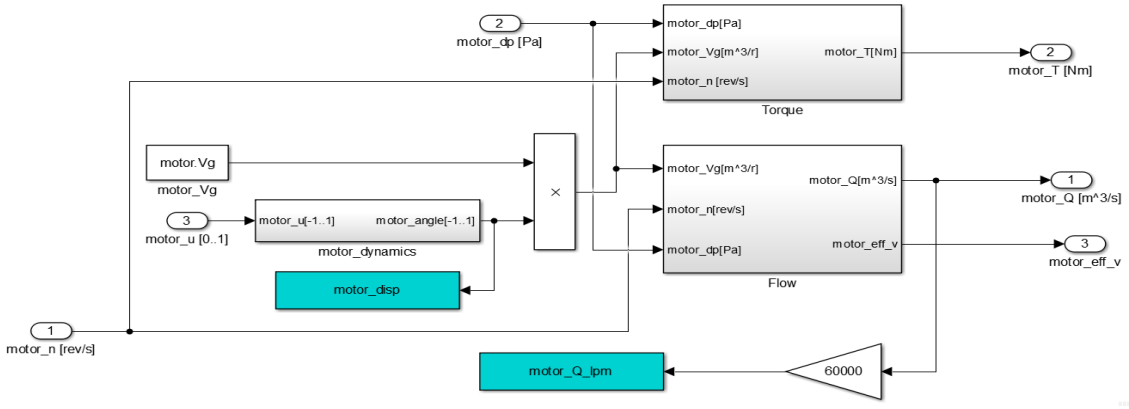

Figure 12. *Simulation model of the hydraulic motor*

Now, the simulation of volumetric flow and torque for hydraulic pump and hydraulic motor, according to equations 2-20 to 2-24, will be illustrated in Figures 13, 14, 15, 16, 17.

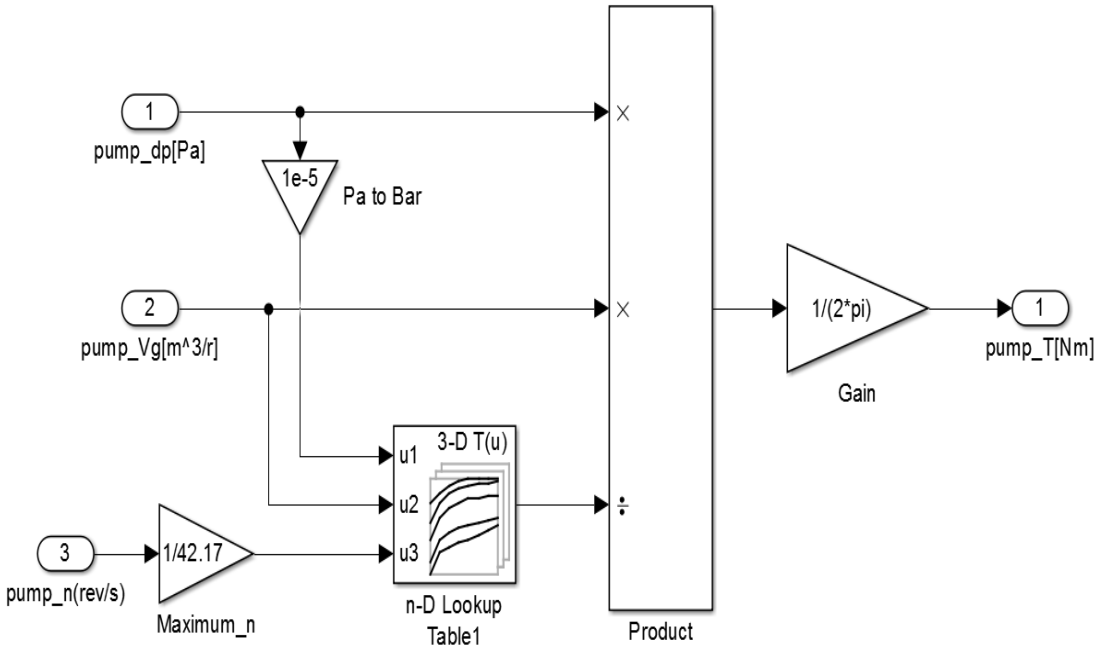

Figure 13. *Simulation model of the boost pump torque*

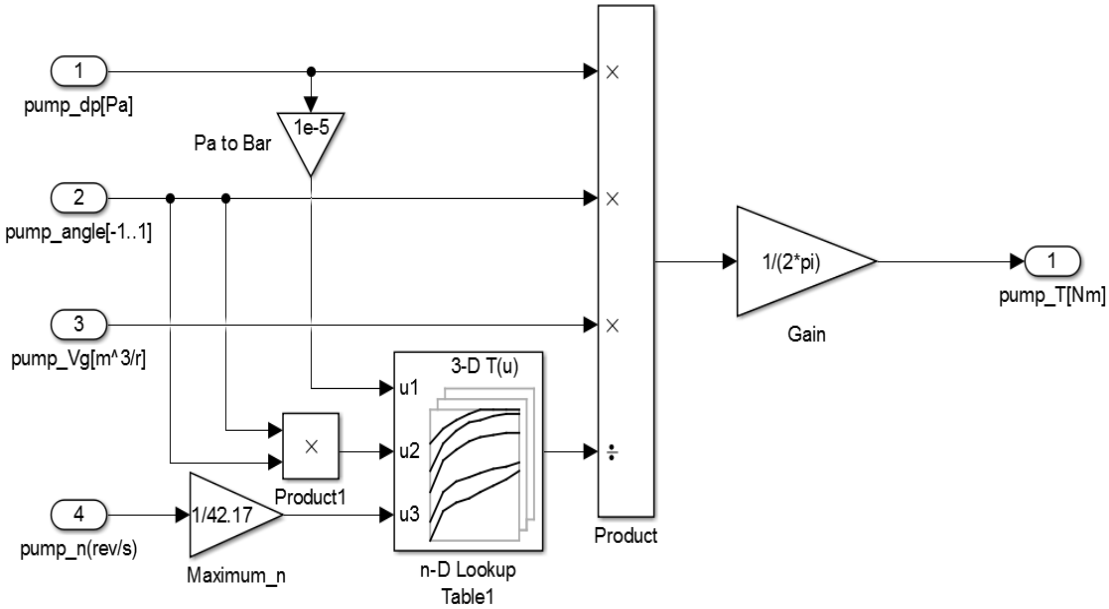

Figure 14. *Simulation model of the hydraulic pump torque*

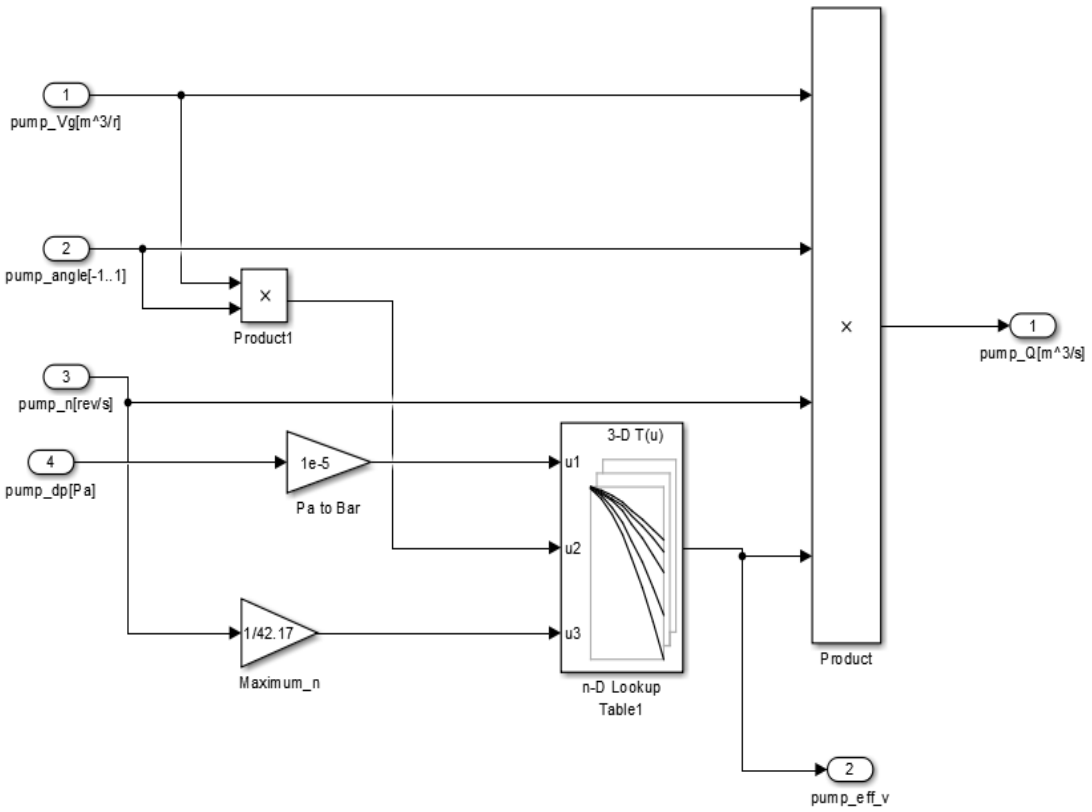

Figure 15. *Simulation model of the volumetric flow of hydraulic pump*

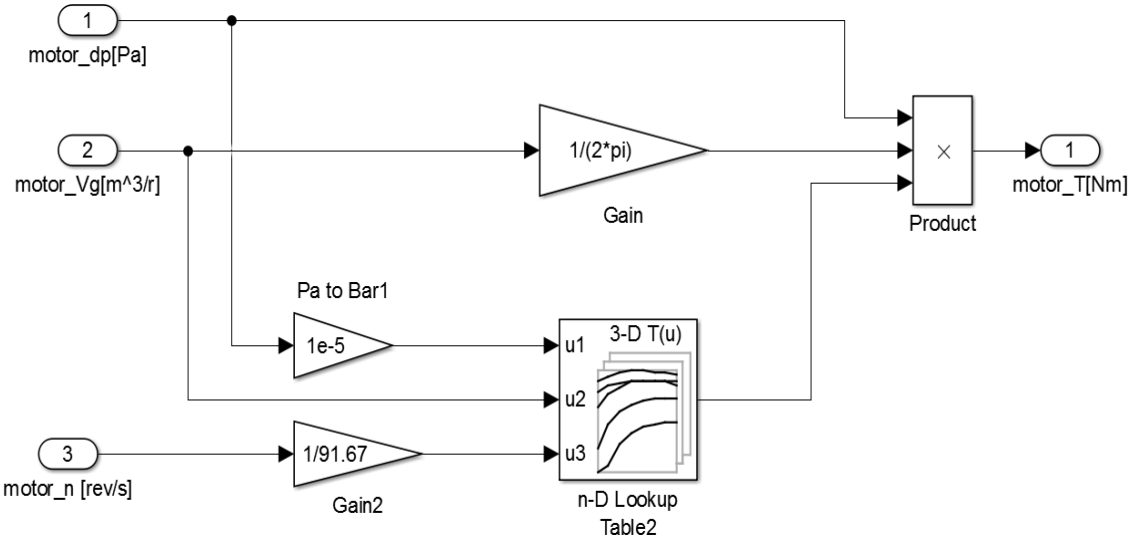

Figure 16. *Simulation model of the hydraulic motor torque*

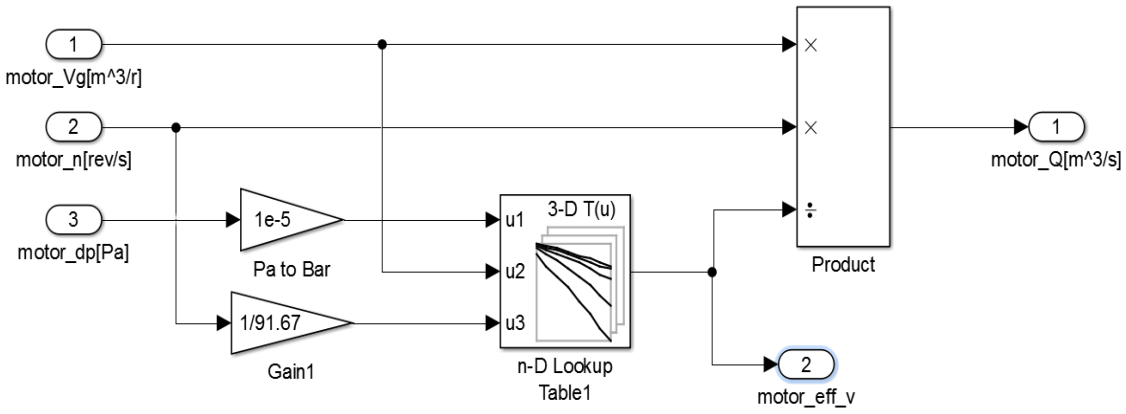

Figure 17. *Simulation model of the volumetric flow of hydraulic motor*

Here, one interesting point should be mentioned. In this modeling, the efficiencies of hydraulic pump and hydraulic motor are not constant, and they vary according to variation of pressure, rotational speed and volumetric displacement. The rotational speed should be implemented in lookup tables as proportional coefficient of maximum rotational speed.

Load

Finally, in the load block, the net force of system (traction force, motor shaft force, and resistant force) leads to the calculation of the rotational speed of the motor. It results in the velocity of the system.

$$\omega_m = \int \frac{\left(T_m - T_l - T_{friction}\right)}{I} \qquad (2-26)$$

In where, the ω_m is the angular velocity of hydraulic motor, T_m is the torque of hydraulic motor, T_l is the torque of the load and $T_{friction}$ is the torque of friction force and I is the inertia of the forwarder. Figure 18 shows the simulation model of load block.

The viscose friction model is shown in Figure 19.

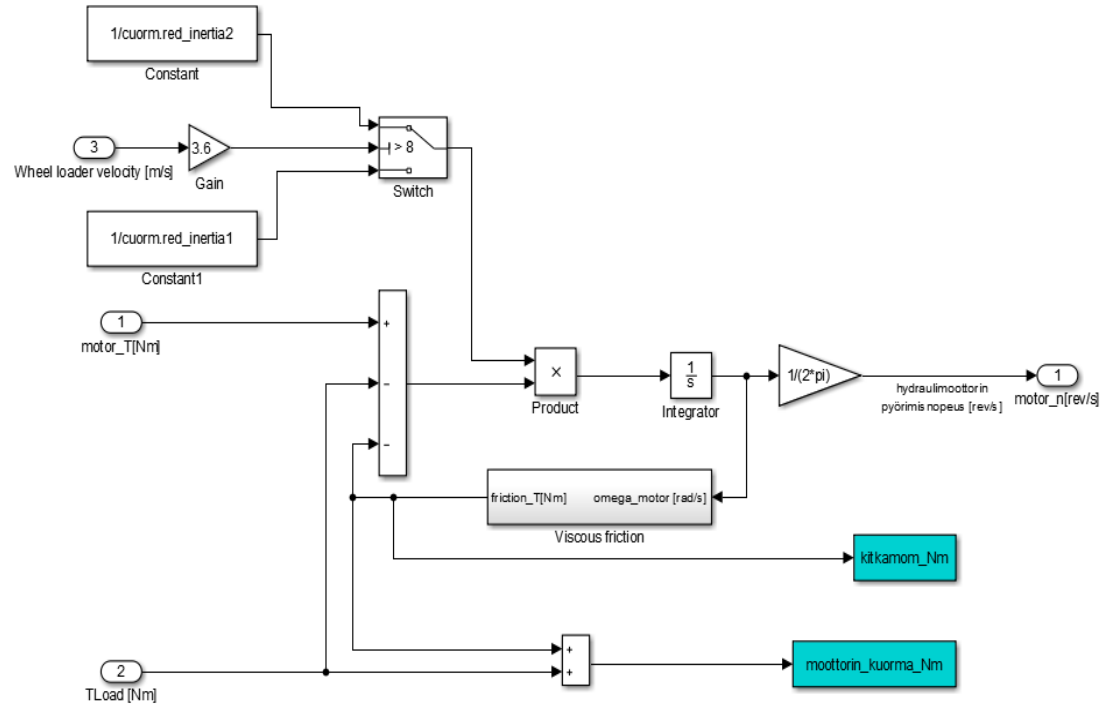

Figure 18. *Simulation model of load*

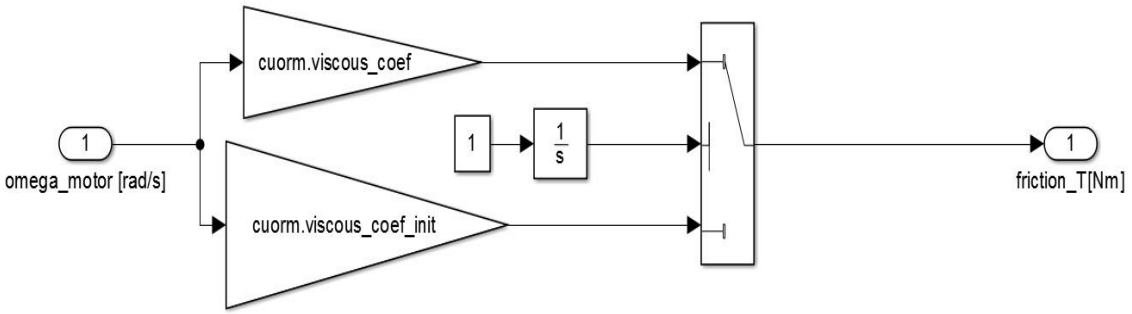

Figure 19. *Simulation model of viscous friction*

2.3 Fuel consumption

In this section, the fuel consumption analyzing will be explained. The calculation is based on the Figure 20 where the fuel consumption has been mapped corresponding to 3 parameters: 1- Relative rotational speed of diesel engine 2- Relative torque of diesel engine 3- relative input power.

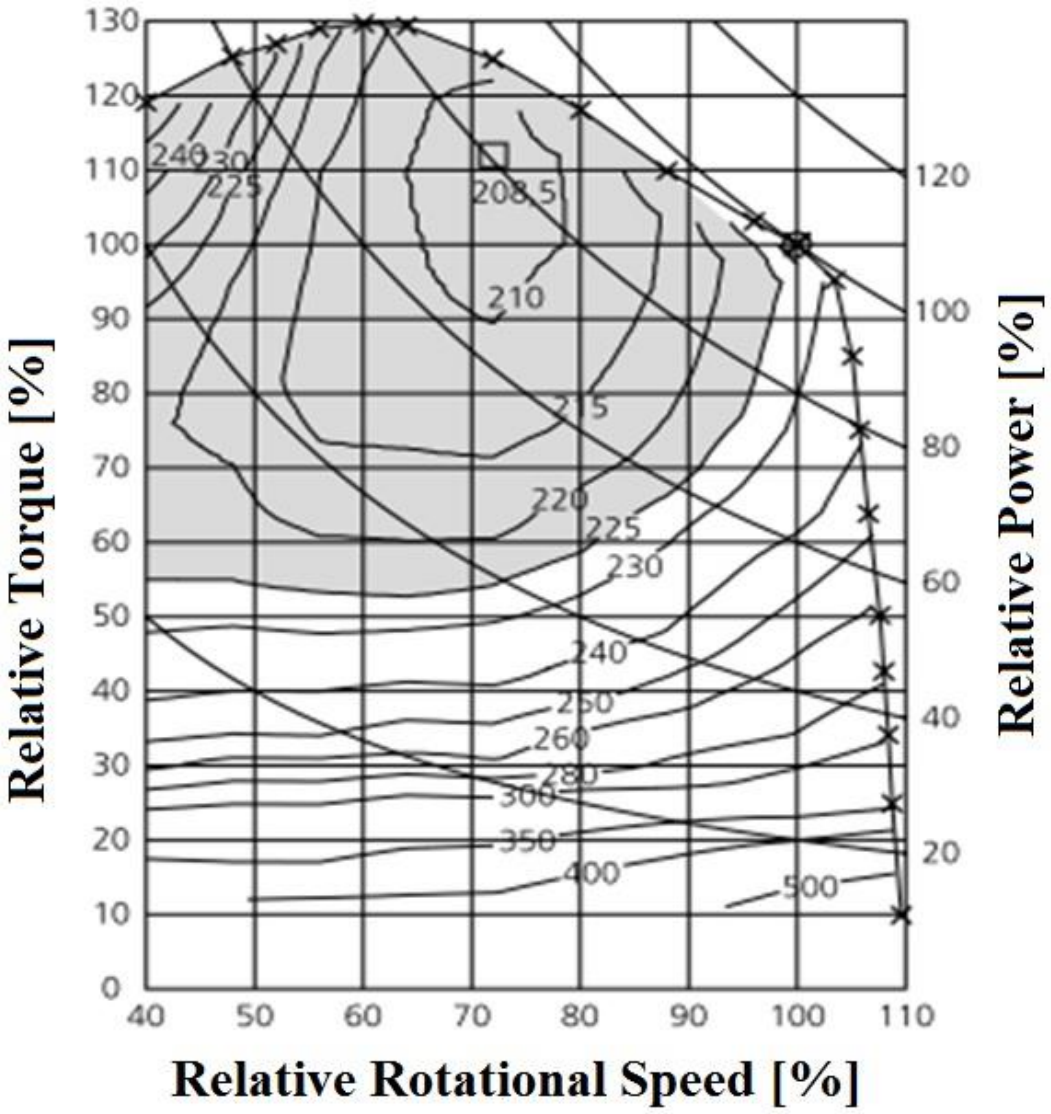

Figure 20. *Fuel consumption map [3]*

Fuel consumption graph will be mapped by neural network and then by using the result of simulation as inputs, the fuel consumption (g/kWh) will be reached.

In neural network, couple of samples (measured inputs and outputs) are selected from the graph or test randomly, depended on the needed accuracy. Then neural network can model the algorithm of these samples and estimate the output of new data based on the algorithm. Usually, the neural network considers the samples in three sequence groups: train (70%), verification (15%) and test (15%).

2.4 Theory of Permanent Magnet Synchronous Motor

In recent years, the PMSM (Permanent Magnet Synchronous Motor) has caught attention considerably due to its applications in industry. It has some significant benefits like high steady state torque density, high performance, and uncomplicated controller of motor

drives which lead to be an appropriate system. By considering the other advantages of PMSM such as low inertia, the small expense of inverter with high reliability in controlling cause engineers to think about its adding in various technical process. [4]

In battery driven PMSM, the battery provides the voltage based on the reference velocity and traction force. In the next step, this voltage produces the currents (direct and quadrature) which causes creation of permanent magnet in rotor. It leads the rotor to rotate with interactive torque.

Generally, the PMSM has two main types: internal-mounted magnets (with saliency, IM) and surface-mounted magnets (without saliency, SM). The most important distinction between them is that IM machine does not have constant reluctance. It means that the reluctance varies with changing the rotational speed. On the other hand, the reluctance is consistent in SM engine. It causes some features such as correspondent air gap, and therefore, the magnetizing inductance will be uniform for both direct and quadrature axis (L_q and L_d) [5]. In the domain of control of PMSM, the Field Oriented Control (FOC) method is famous which will be used this project.

Before explaining the detail of PMSM, it should be emphasized that this chapter is coincided with reference [6]. The schematic of PMSM system is demonstrated in Figure 21.

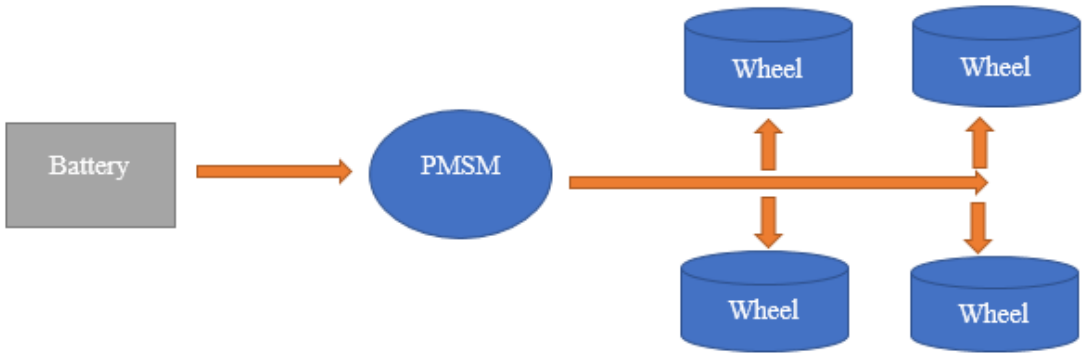

Figure 21. *PMSM schematic*

Due to avoiding computational complexity, the surface-mounted synchronous model of PMSM will be implemented in this project work. A cross-section for rotor and stator detail is shown in Figure 22. In three-phase PMSM modeling, by the assumption of two poles in d-q domain, the voltage can be gained with below equation [5]:

$$\overrightarrow{u_{dqos}} = R_s * \overrightarrow{i_{dqos}} + p.\overrightarrow{\lambda_{dqos}} \qquad (2-27)$$

p is the sign of the differentiation operator $\frac{d}{dt}$. The various axes, indicated by d, q and 0, are direct axis, quadrature axis, and zero component of variables respectively. The flux linkage can be gained by below equations:

$$\overrightarrow{\lambda_{dqos}} = L_{dq} * \overrightarrow{\iota_{dqos}} + \overrightarrow{\lambda_{dqom}} \qquad (2-28)$$

in continue, the inductance matrix can be displayed:

$$L_{dqo} = \begin{bmatrix} L_d & 0 & 0 \\ 0 & L_d & 0 \\ 0 & 0 & L_o \end{bmatrix} = \begin{bmatrix} L_s & 0 & 0 \\ 0 & L_s & 0 \\ 0 & 0 & L_o \end{bmatrix} \qquad (2-29)$$

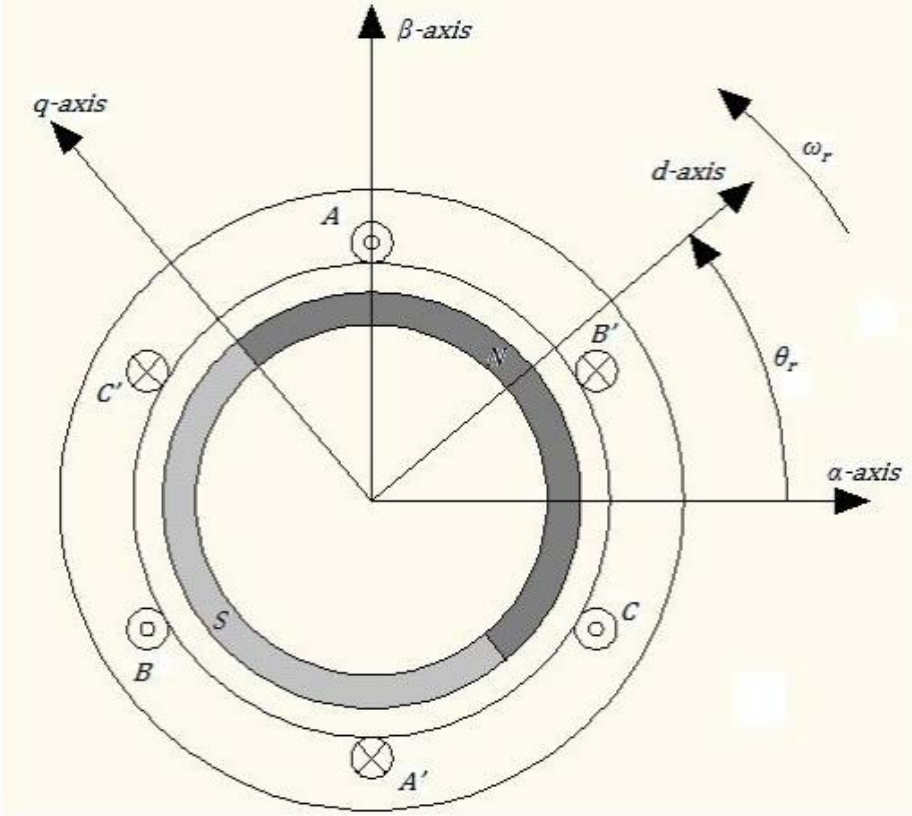

Figure 22. *View of three-phase, two-pole PMSM [6]*

As it was mentioned before, the inductances are equal in d and q direction. The s notation is related to the stator. So, the magnetic flux can be presented in below format:

$$\lambda_{dqom} = [\lambda_{pm} \quad 0 \quad 0]^T \qquad (2-30)$$

By considering the stator windings that are eye-connected and provided with equitable three-phase currents, therefore, the zero axis components can be ignored [5]. It causes the voltage equations for d and q direction will modify to below equation:

$$u_{ds} = R_s * \ i_{ds} + L_s * \frac{di_{ds}}{dt} - \omega_r * L_s * i_{qs} \qquad (2-31)$$

$$u_{qs} = R_s * \ i_{qs} + L_s * \frac{di_{qs}}{dt} + \omega_r * \left(L_s * i_{ds} + \lambda_{pm}\right) \qquad (2-32)$$

R_s is stator resistance, L_s the stator inductance, ω_r the rotor rotational speed and λ_{pm} the permanent magnet flux. Now, the electromagnetic torque can be calculated as below:

$$T_e = \left(\frac{3}{2}\right) * \left(\frac{p}{2}\right) * \left(\lambda_{ds} * i_{qs} - \lambda_{qs} * i_{ds}\right) \qquad (2-33)$$

by replacing the equation (2-28), the latest version of electromagnetic torque can be obtained:

$$T_e = \left(\frac{3}{2}\right) * \left(\frac{p}{2}\right) * \left(\lambda_{pm} * i_{qs} - (L_q - L_d) * i_{qs} * i_{ds}\right) \qquad (2-34)$$

Because the inductances are the same:

$$T_e = \left(\frac{3}{2}\right) * \left(\frac{p}{2}\right) * \left(\lambda_{pm} * i_{qs}\right) \qquad (2-35)$$

This important sequence means that just stator q-axis current is required to produce torque.

2.5 Field Oriented Control theory

At the first part of this chapter, it was mentioned that Field Oriented Control method is one the modern vector control method in PMSM topic. In this approach, the controlling of magnetic field and torque is the primary objective by controlling the stator currents and flux linkage in both d and q direction effectively. The system response in this method is rapid, and moreover, the torque ripple is tiny [7]. As it can be seen in Figure 23, the currents in both direction and angular velocity are inputs.

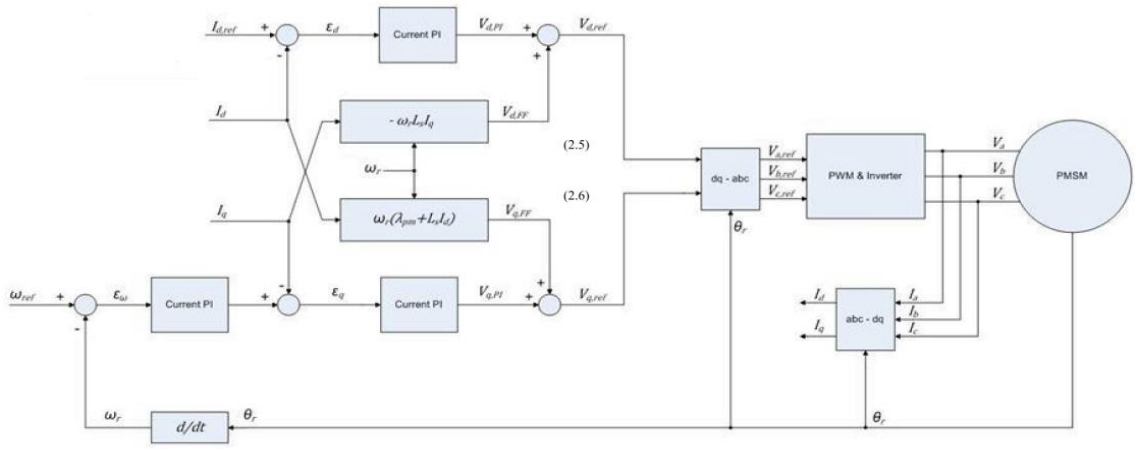

Figure 23. *Diagram of the implemented FOC [6]*

In Figure 23, there are three controllers: one for the mechanical system which compares the reference speed with measured one then, this difference is fed into the PI controller, and the output will be torque command. The second and third controllers are related to electrical systems (id and iq currents):

$$\frac{d\omega_r}{dt} = \frac{1}{J} * (T_e - T_m - B * \omega_r) \qquad (2-36)$$

In this equation J is inertia of the motor, B is viscous coefficient, T_m is mechanical torque (load), applied by the mechanical system and T_e is the electrical load which produces by PMSM. There is one critical issue about PI controller for stator current in d direction. The reference value for it is zero due to not existing flux weakening. Another electrical controller tunes the current in q direction and compare it with measured q current and then, feeds it.

Equations 2-31 and 2-32 have been implemented as feedforward compensation in PI controller to improve the performances. In these two controllers, the $V_d$and V_q are outputs, converted to abc domain firstly by using the Park and Clark transformation (Appendix A). In the next step, they will be used in PWM unit to produce the command signal for the inverter. Below method will be implemented order to adjust the PI controller [8].

$$\alpha_{current} = \frac{2 * \pi * f_s}{10} \qquad (2-37)$$

$$\alpha_{speed} = \frac{\alpha_{current}}{10} \qquad (2-38)$$

$$K_{pd} = \alpha_{current} * L_d \qquad (2-39)$$

$$K_{Id} = \alpha_{current} * R_s \qquad (2-40)$$

$$K_{pq} = \alpha_{current} * L_q \quad (2-41)$$

$$K_{Iq} = \alpha_{current} * R_s \quad (2-42)$$

$$K_{P\omega} = \alpha_{speed} * J \quad (2-43)$$

$$K_{I\omega} = \alpha_{current} * B \quad (2-44)$$

where $\alpha_{current}$ and α_{speed} are bandwidths of controllers, and the switching frequency of the inverter, defined by f_s which is equal to sample frequency of the system.

the primary task of these controller coefficients is keeping the torque and voltage value in the legal limitations. Therefore, the saturation blocks will be added to the simulation model to prevent overshooting the maximum amounts. This issue leads to a major problem, a significant exceeding in current value due to wind up phenomena. While the output voltage has the highest level, it holds the error high. Simultaneously, when the current reaches the highest amount, the integrator function is wound up. Therefore, the voltage keeps its maximum.

Anti-winding approach can be utilized to avoid the problem. In this method, the integral term of the controller should be renewed by reference torque or voltage. While the voltage command is lower than the maximum, the anti-windup passes zero value to the integrator. But when this amount is exceeded, the comparative value of this variation is appended to the integrator, so the response of controller will be quicker. Later, the effect of this process on simulation will be illustrated.

Briefly, the FOC block diagram performance can be reviewed in below steps:

1- The measured elements are stator current and rotor angle.

2- The Clark Transformation causes the stator currents to convert into a two-axis reference frame.

3- The Park Transformation leads to alpha - beta currents to switch into rotor reference frame. These currents are constant under steady-state conditions.

4-The d-current checked the air gap flux, at the same time, the q current restrains the torque. Lastly, the quadrature-axis current reference can be computed by the speed controller

5- the reference voltage can be generated by current error signals which are implemented in the controller.

6- Then, the reference voltage is returned to abc domain.

7- Finally, the reference voltage which is calculated by the PWM, will be utilized for driving the inverter.

2.6 Simulation of PMSM

In this section, the simulation of PMSM will be explained according to defined theories. Figure 24 shows the general view of PMSM simulation where there are four blocks: 1- Controller Synchronization, 2- $d-q$ to $\alpha-\beta$ 3- PWM inverter 4- IPM PMSM model. In the following parts, these blocks will be described in detail, and all related functions will be defined.

2.6.1 Controller Synchronization

In Figure 25, the Controller Synchronization block is shown where the reference velocity, id ref (which is equal to zero), measured i_d and measured i_q are inputs. All Three PI controllers can be observed, two PI controllers for i_d and i_q and the speed controller. The feedforwards compensations are based on equations 2-31 and 2-32 and all control coefficients have been defined in (2-37…2-44). Anti-windup controllers are also can be recognized which adjust the integrator values.

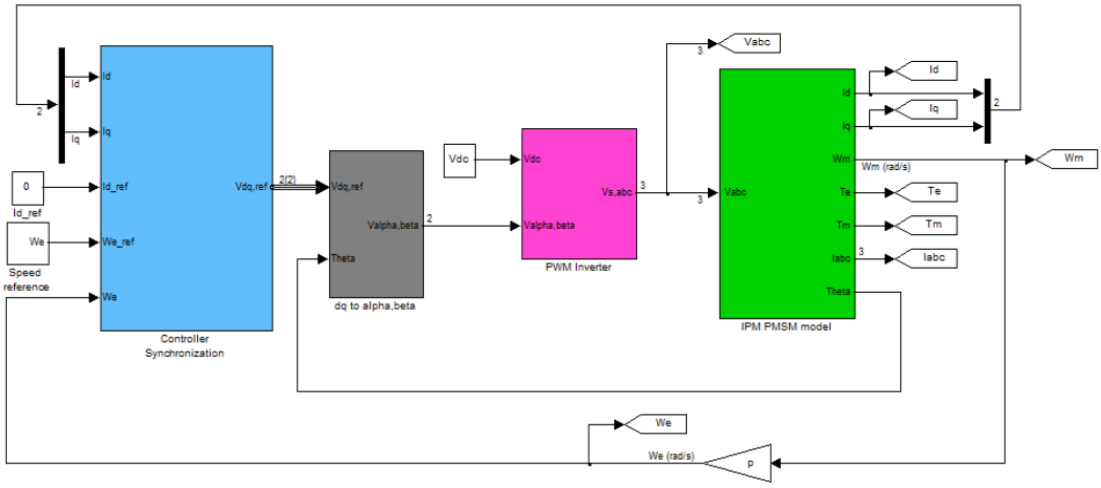

Figure 24. *The general view of PMSM simulation*

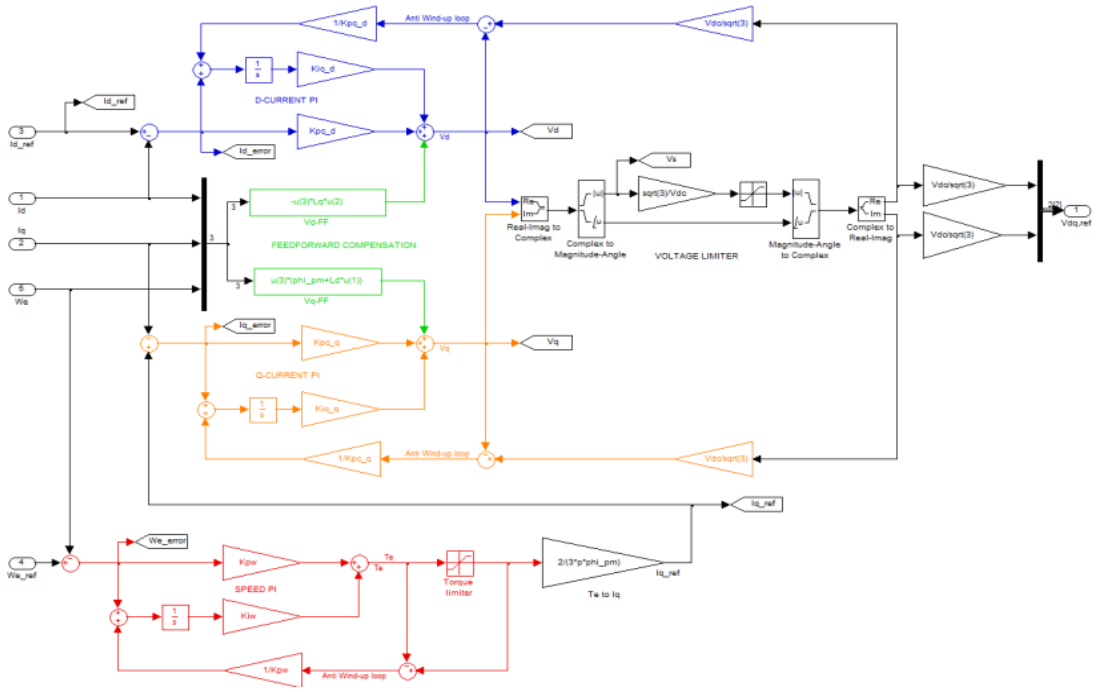

Figure 25. *Simulation model of controller synchronization*

2.6.2 The $d-q$ to $\alpha-b$ voltage converter

In Figure 26, the mathematical model for converting the reference voltage from $d-q$ frame to $\alpha-b$ frame represents:

$$V_{dq\to\alpha\beta} = \begin{bmatrix} \cos\theta_r & -\sin\theta_r \\ \sin\theta_r & \cos\theta_r \end{bmatrix} \qquad (2-45)$$

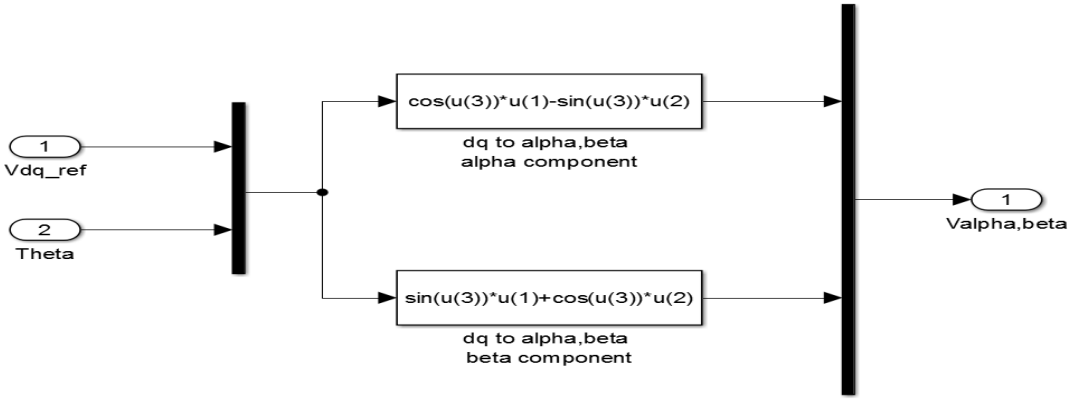

Figure 26. *$d-q$ to $\alpha-\beta$ voltage converter*

2.6.3 PWM converter

Figure 27 is about the V_{dc} inverter where one switch is used for each phase to set the V_{dc} or $-V_{dc}$. The switch changes the phase corresponding to S_{abc} which is produced in PWM generator, and its value is between 0 and 1. Figure 28 shows the detail of PWM generator.

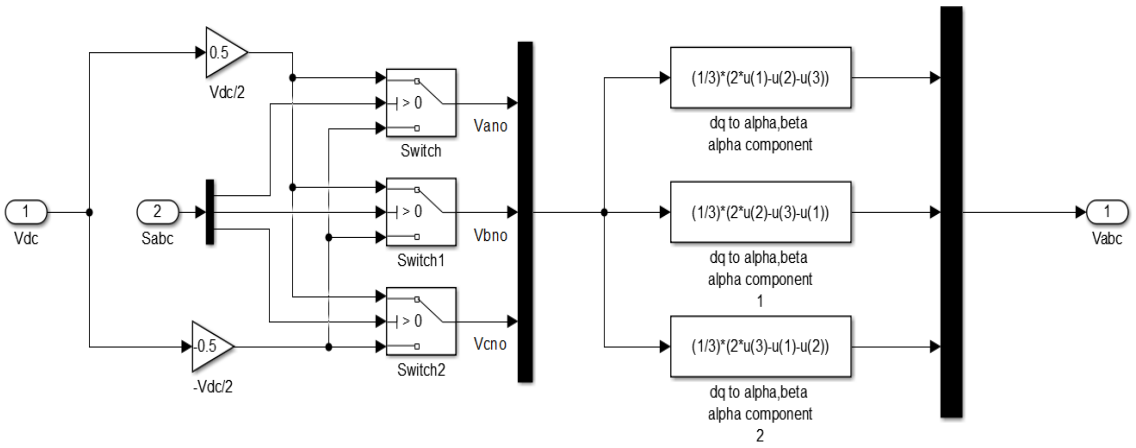

Figure 27. *The voltage inverter*

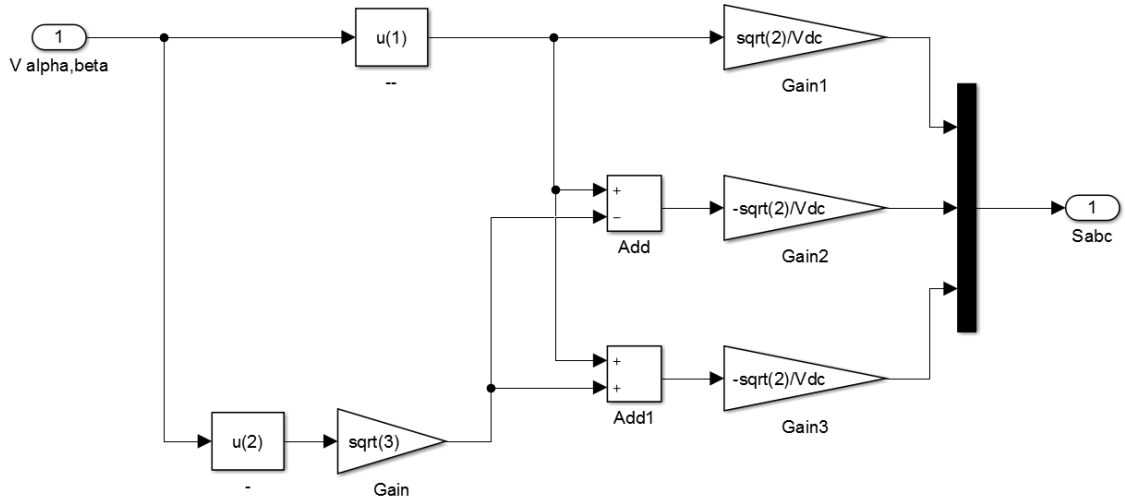

Figure 28. *PWM generator*

2.6.4 IPM PMSM

IPM PMSM simulation describes in Figure 29 that has two sub-blocks. In converter block, the reference voltage in $a-b-c$ frame should convert to $d-q$ frame with following mathematical equation:

$$V_{abc-dq} = \begin{bmatrix} \cos\theta_r & \cos\left(\theta_r - \frac{2\pi}{3}\right) & \cos\left(\theta_r + \frac{2\pi}{3}\right) \\ -\sin\theta_r & -\sin\left(\theta_r - \frac{2\pi}{3}\right) & -\sin\left(\theta_r + \frac{2\pi}{3}\right) \end{bmatrix} \quad (2-46)$$

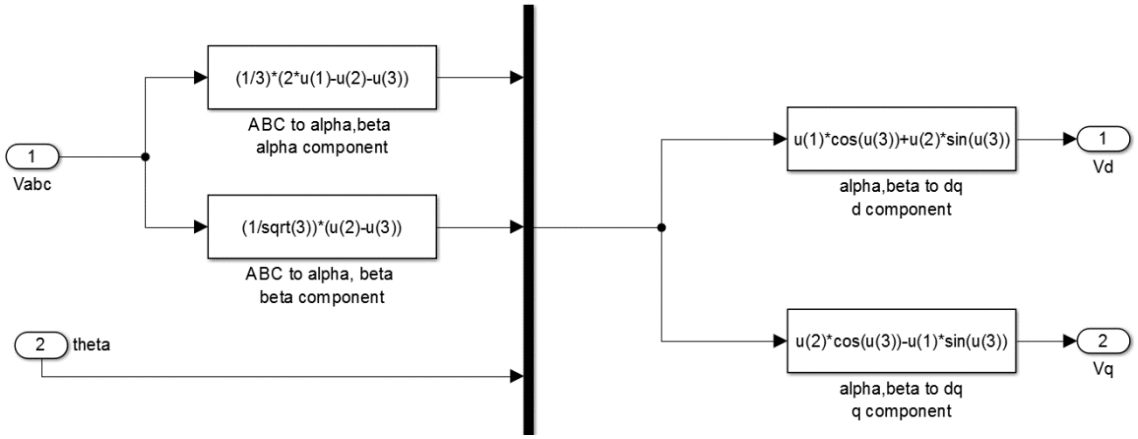

Figure 29. *Clark & Park reference frame conversion (direct)*

Then, V_{dq}will be sent to PMSM simulation as inputs. Mechanical equation (2-46) produces the angular velocity, and the measured i_d and i_q are computed by equation (2-31) and (2-32) respectively. These measured values are sent to the controller block to compare with references. Figure 30 shows the detail of PMSM simulation.

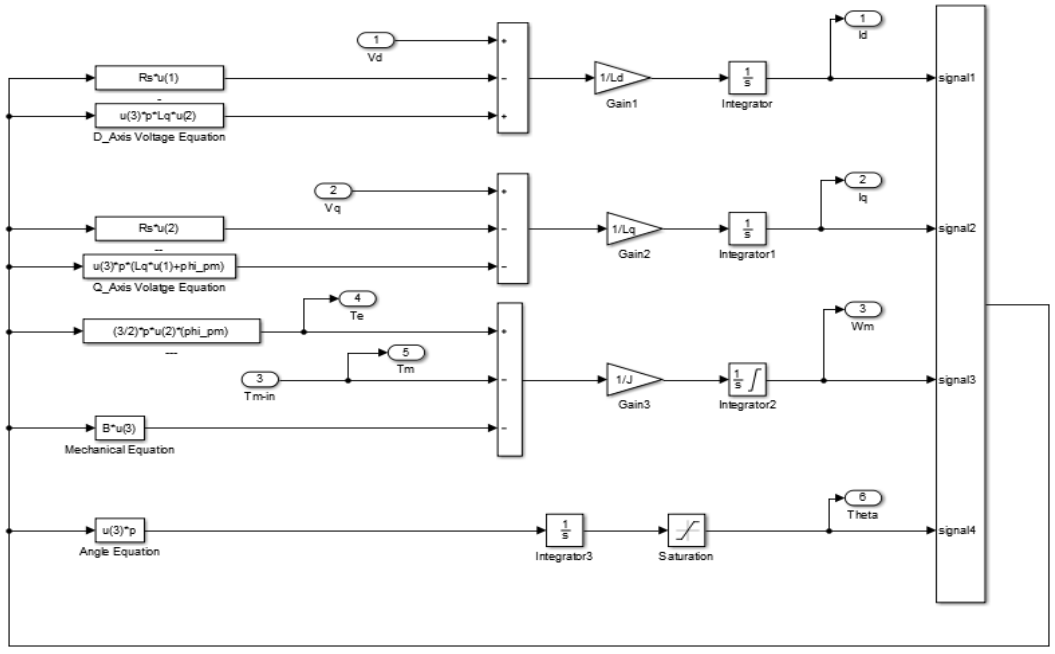

Figure 30. *Simulation model of IPM PMSM*

To nutshell, the theory of PMSM model has been explained firstly and then all mathematical equations, used in simulation blocks, has been defined. Next, the simulation blocks have been demonstrated. In the next chapter, the result of hydromechanical and electrohydraulic will be analyzed.

2.6.5 PMSM efficiency

In order to calculate the PMSM efficiency, the torque – rotational speed graph has been implemented (Figure 31). Like fuel consumption, this figure has been mapped in simulation file by neural network method.

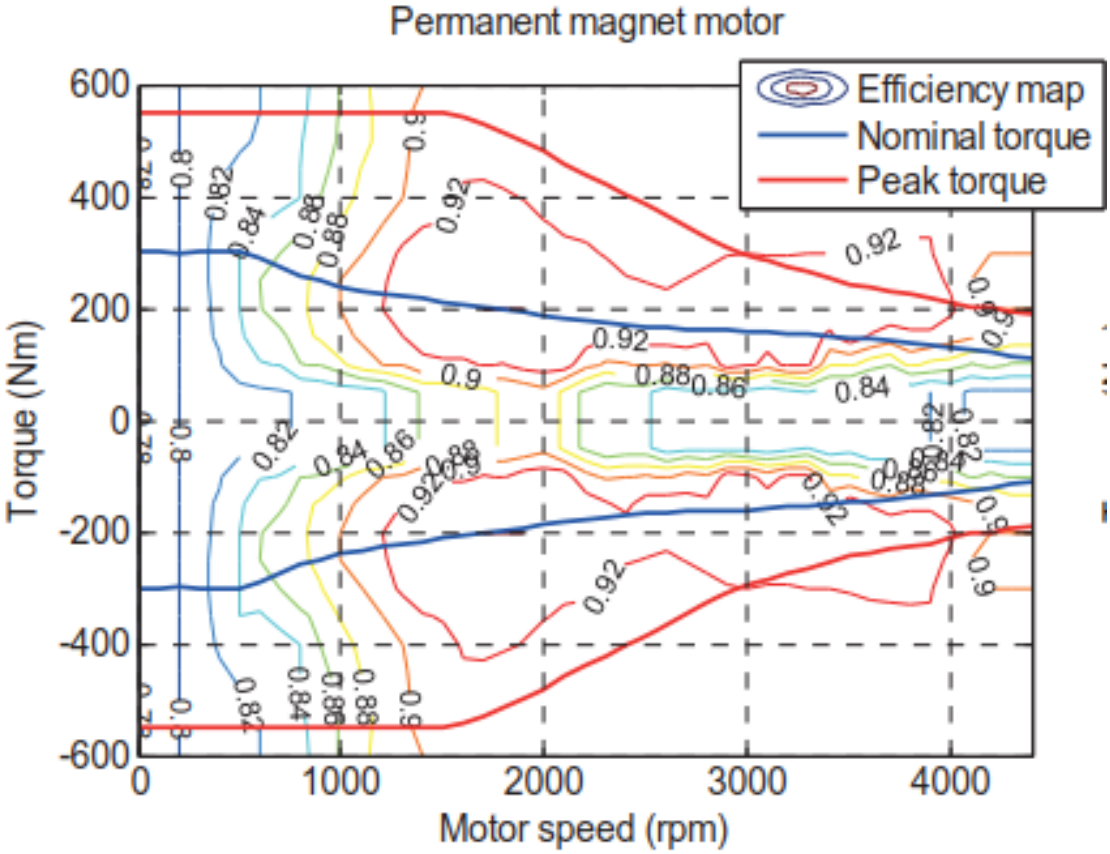

Figure 31. *Efficiency map according to PMSM torque and rotational speed [9]*

3. RESULTS AND CONCLUSIONS

After reviewing the theories and Simulink models of driveline and PMSM, the conclusive results and their analysis will be demonstrated in this chapter. Their parameters and initial equations have been implemented in MATLAB Mfile.

3.1 Results of driveline simulation

As it was mentioned earlier, the drive line simulation has been implemented to achieve one specified goal: following the velocity trend in two speed ranges: between 0 and 8 km/h and between 0 and 27 km/h. According to Corner Power Theory and by using the drive line functions, the traction forces and velocities should be assigned in point 1 and point 2. Duo to avoiding tedious explanations, the detailed calculations have been provided in the appendix and here just the figures will be evaluated.

3.1.1 Low speed range

In low speed range, the gear ratio is 92. The traction force and velocity in point 1 are 130 kN and 2 km/h respectively, and in point 2, they are 31.9 kN and 8 km/h.

In Figure 32, the result of simulation for traction force and motor force is represented in where the reference and filtered traction forces, and simulated motor force have been modeled. The variation between the reference and filtered force is due to delay in effect of gas pedal on the system. The difference between filtered traction force and simulated motor force is lower than 10% before second 30 and then, it grows around 15% slowly because of smooth increasing of velocity which means more hydraulic torque.

Figure 33 shows the result of velocity simulation in where the reference, filtered, and simulated velocities have been compared. Similarly, the difference between the reference and filtered is because of delay in the gas pedal set value. The difference between the filtered and simulated speeds is negligible until second 45, then, the difference increases near 10% gradually.

Figure 34 is about the controlling the hydraulic pump and motor displacements. The displacement of hydraulic pump rises to the maximum value at second 19.5 and next, the motor displacement goes down. Between seconds 10 and 15, the velocity is constant; consequently, the pump displacement remains steady approximately and then, it goes up by increasing the speed. The minimum relative value of hydraulic motor displacement is 33%.

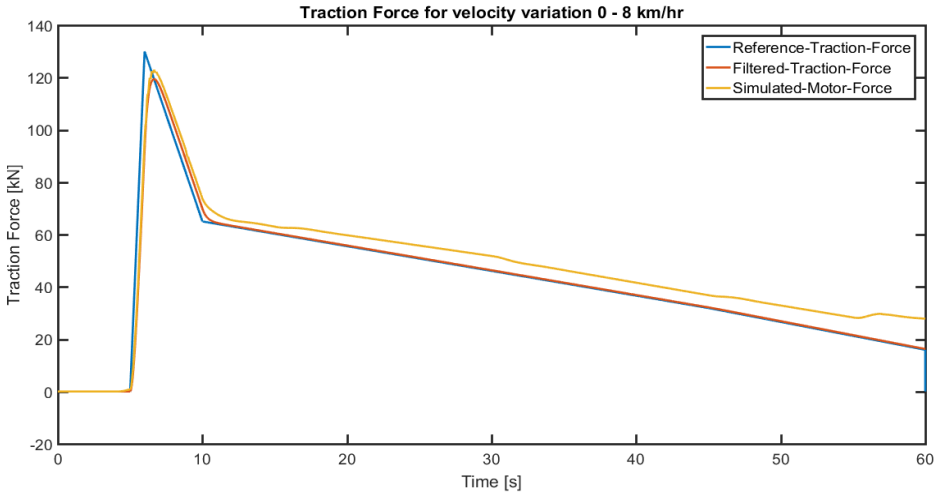

Figure 32. *The traction forces and simulated motor force trend*

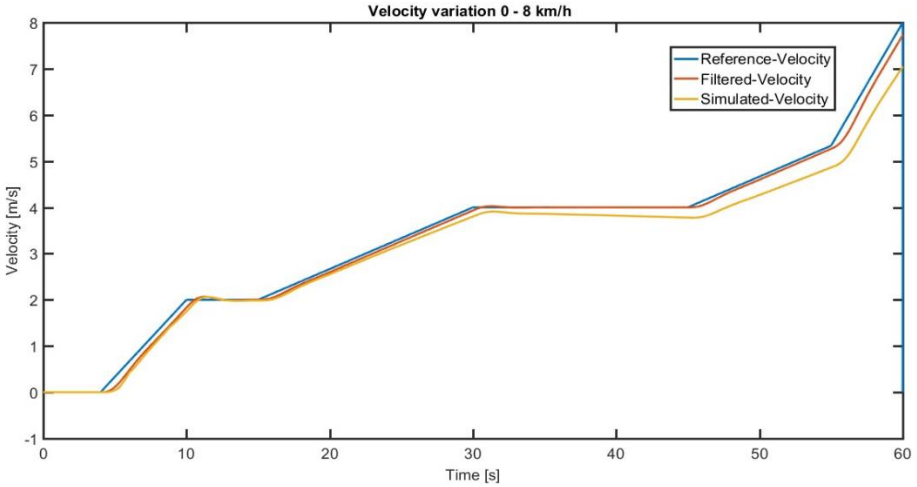

Figure 33. *The reference, filtered and simulated velocities trend*

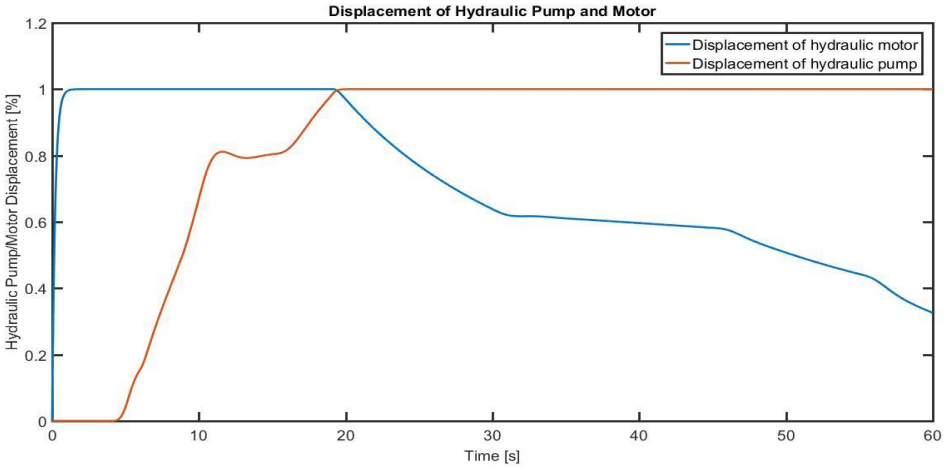

Figure 34. *Hydraulic pump and motor displacement*

One of the key features of modeling in this research is that the efficiencies are not constant, and they vary according to pressure, rotational speed, and displacements. Figure 35 illustrates the efficiencies fluctuations during the simulation period. Obviously, the traction force has paradox effects on efficiencies; its ascending causes the mechanical efficiencies to increase about 10%. On the other hand, it leads to decline the volumetric efficiencies 5%. Next, the velocity trend does not have the significant effect on pump efficiencies while motor efficiencies reduce 8%. It should be mentioned that the efficiencies in first 5 seconds were not calculated correctly due to zero velocity and zero traction force.

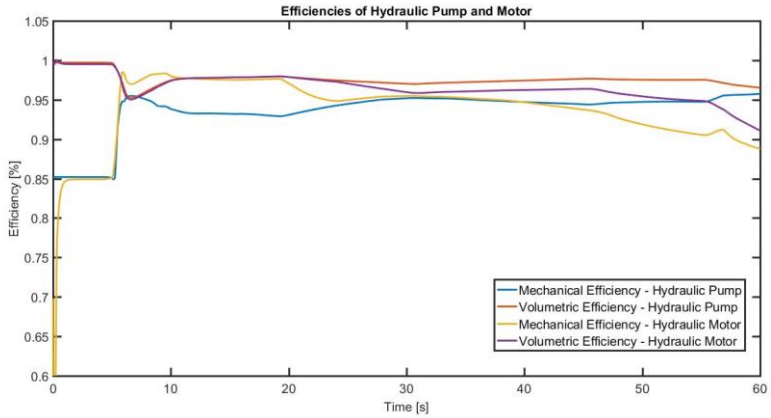

Figure 35. *Volumetric and Mechanical efficiencies.*

The pressure fluctuation of the hydraulic system is shown in Figure 36. It reaches the maximum level (310 bars) due to high traction force at the first moments. The speed does not influence considerably on the pressure even its constant trend causes the pressure fallen. in the maximum velocity, the pressure is the 237 bars.

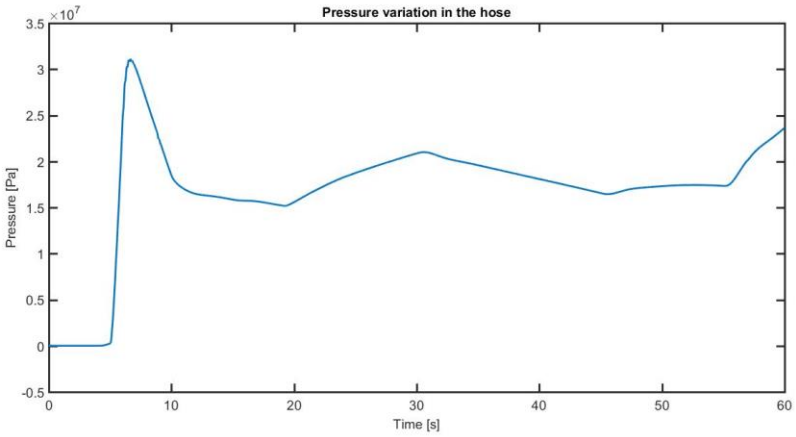

Figure 36. *Pressure fluctuation*

In Figure 37, the power of diesel engine is shown. The traction force increases the pressure of the systems dramatically. Then increasing the velocity leads to higher pressure level. The pressure has descending trend just when the velocity is invariable.

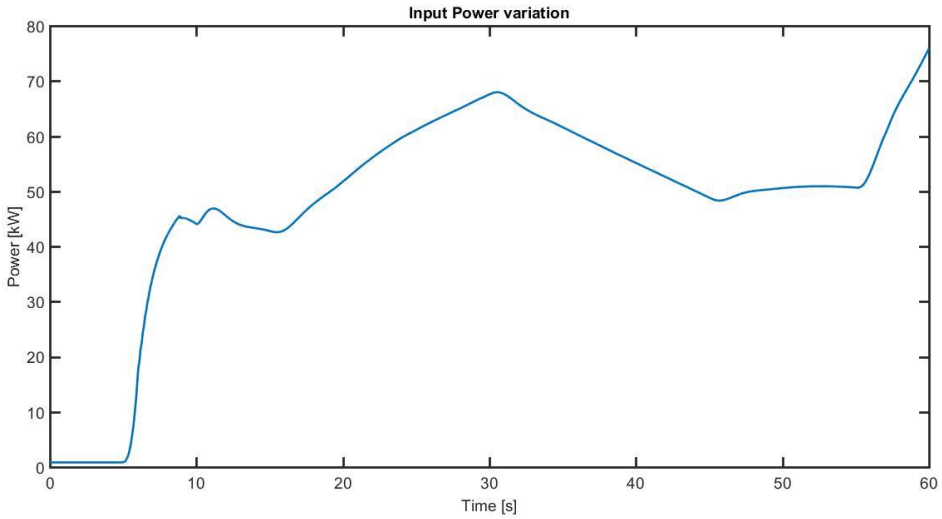

Figure 37. *Input (diesel engine) power*

In Figure 38, the fuel consumption of diesel engine is illustrated. In the first moments, fuel consuming is rather high 530 (g/kWh) then, it declines 55% due to increasing the traction force and next, fuel consumption trend proves that the increasing of velocity reduces it again from 230 and 217 (g/kWh). It also should be mention that constant velocity leads to ascending consumption trends because of dropping of diesel power.

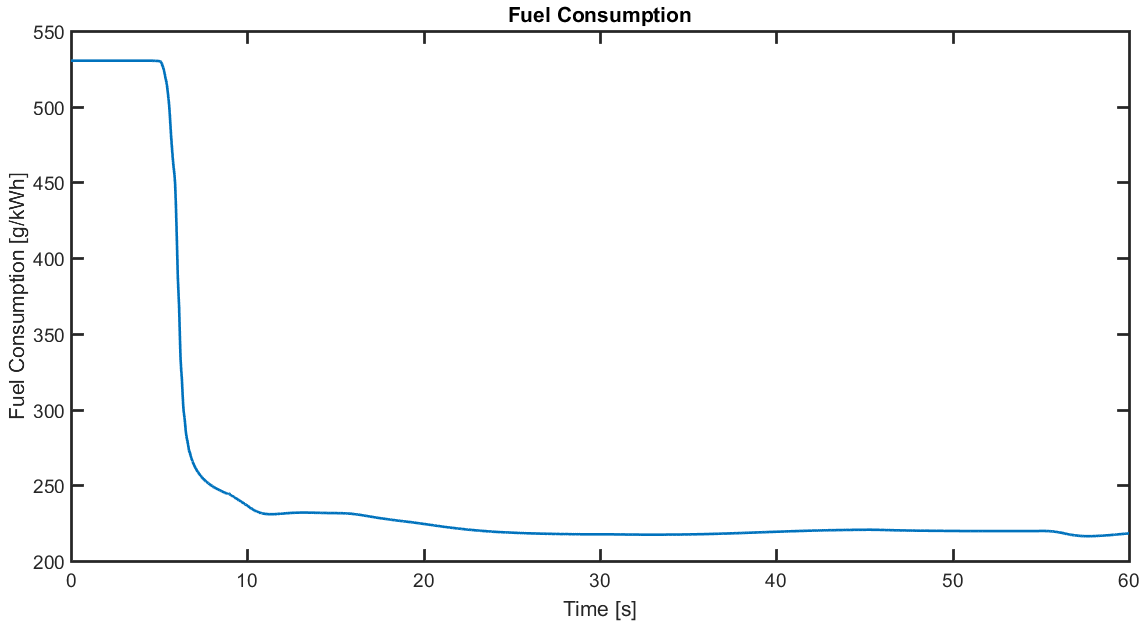

Figure 38. *Fuel Consumption of diesel engine – velocity in range 0-8 km/h*

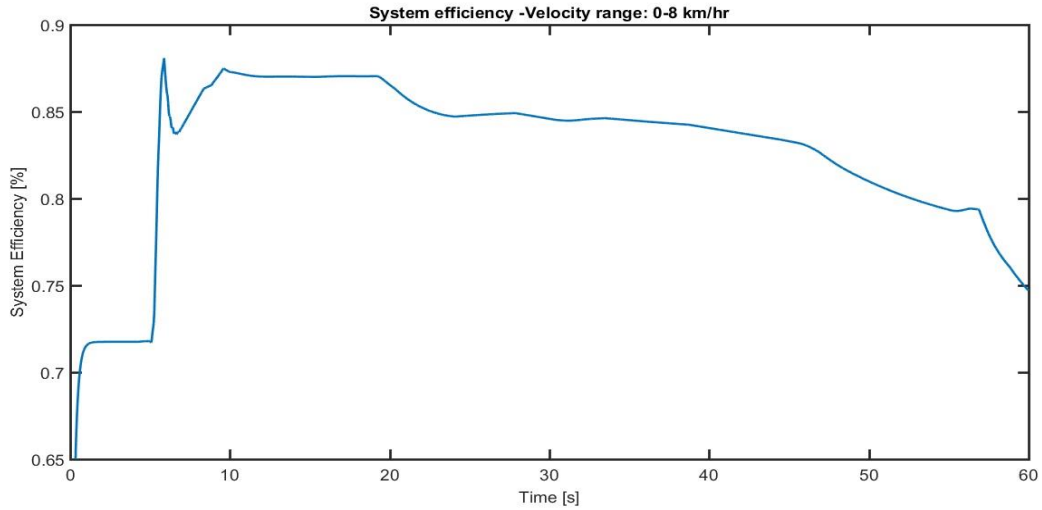

Figure 39. *The total efficiency of hydromechanical system*

Figure 39 shows the total efficiency of the hydromechanical system. Until second 20, the efficiency is around 87% and then, it goes down to 75%. Reduction the motor efficiencies (specially the mechanical efficiency) is the main reason of this descending trend.

3.1.2 High speed range

When it is supposed to increase the maximum speed in the model, the gear ratio should be reduced, therefore, the system cannot handle the high traction force. In the high speed range, the maximum velocity became three times more, so the gear ratio is divided by three (the gear ratio is 35). Similarly, the traction forces and velocities were calculated based on Corner Power Theory. In the point 1, the maximum force was assigned to 45 kN, and the calculated velocity is 1.5 km/h. In the point 2, the traction force and velocity are 9,5 kN and 27 km/h respectively.

In Figure 40, the reference and filter traction force, and simulated motor forces are demonstrated. Until second 20, the simulated motor force can follow the filtered one correctly due to low speed range. After that time, because the velocity goes in couple of time intervals (acceleration), it results increasing of motor force, especially after second 60 where the velocity reaches 27 km/h.

Figure 41 shows the trend of reference, filtered, and simulated velocities. Apparently, the simulated speed can follow the filtered one rightly, and their difference is constant all the time. It means that although the error was around 20% between seconds 30 and 40, it declined to about 10% after second 70.

Figure 42 relates to controlling the hydraulic pump and motor displacement. The displacement of hydraulic pump reaches the maximum at second 26, and then the fluctuation of the motor displacement has the biggest effect on to increase the velocity. The smallest hydraulic motor displacement is 31%.

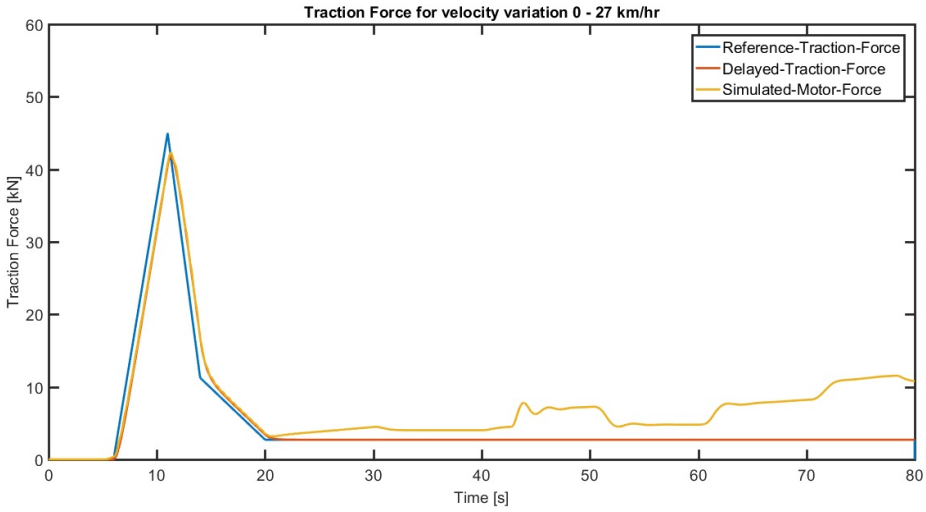

Figure 40. *The traction forces and simulated motor force trend*

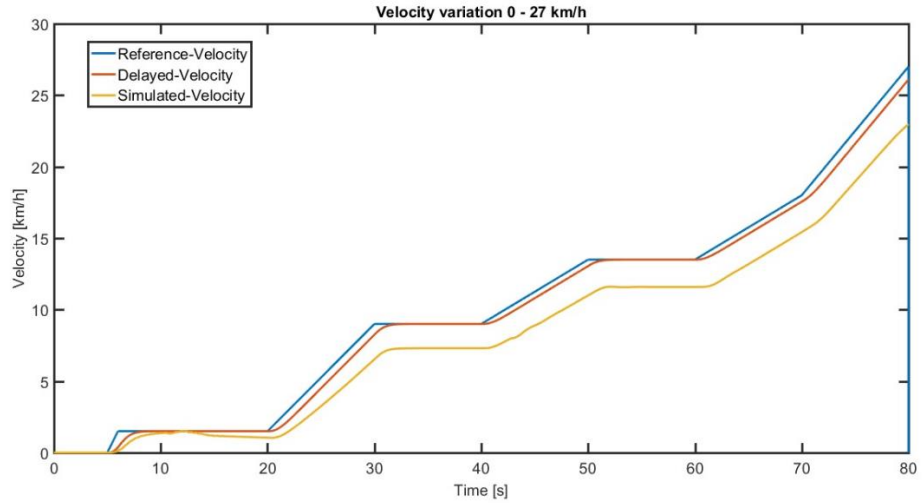

Figure 41. *The reference, filtered and simulated velocities trend*

Like Figure 35, the efficiencies fluctuations are illustrated in Figure 43. Although the effect of traction force is exactly analogous to the previous condition in the first 20 seconds (increases the mechanical efficiencies near 10 %), the higher velocity amount and its bigger variations lead to important influences on performances. When the velocity has raising trend, the mechanical efficiency of pump increased around 10 % and similarly, the mechanical efficiency of motor raised about 5%. Simultaneously, the volumetric efficiencies of pump and motor reduced 3% and 8% respectively. It should be mentioned that the constant speed causes decreasing the mechanical efficiencies around 5%.

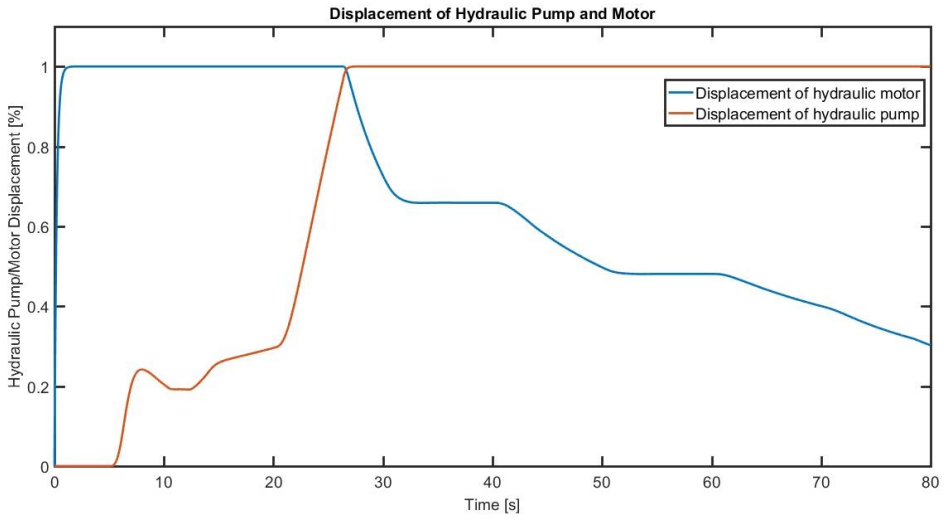

Figure 42. *Hydraulic pump and motor displacement*

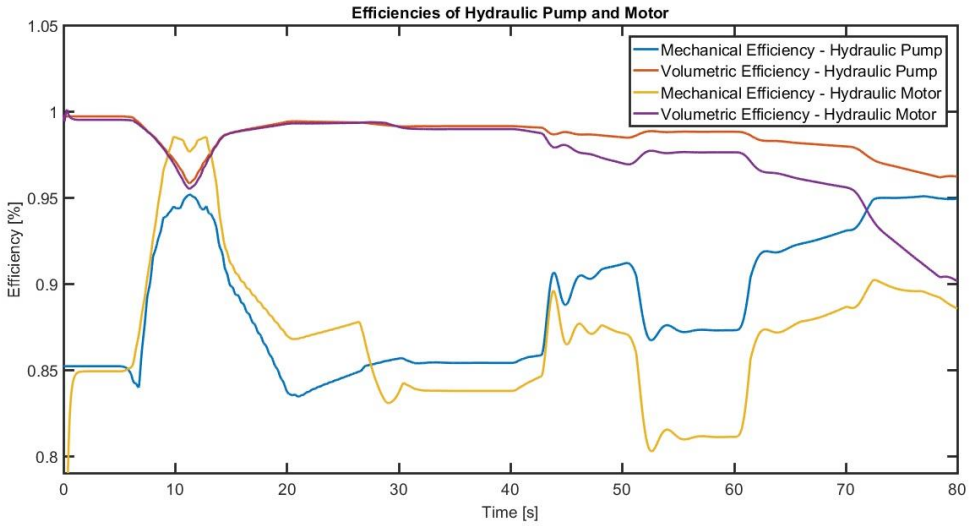

Figure 43. *Volumetric and Mechanical Efficiencies*

Figure 44 shows the change of pressure during the simulation time. Because the traction force was limited noticeably, the pressure goes up just near 280 bars (in the low range speed, it reached the maximum pressure level 340 bars). Next, the trend of velocity led to increasing the pressure to around 252 bars (like the previous condition)

In Figure 45, the used power of diesel engine is shown where due to the higher speed than the former condition, the more power has been consumed. In the previous condition the maximum power was 76 kW while in this one, it reached the 98 kW which the maximum capacity of the diesel engine.

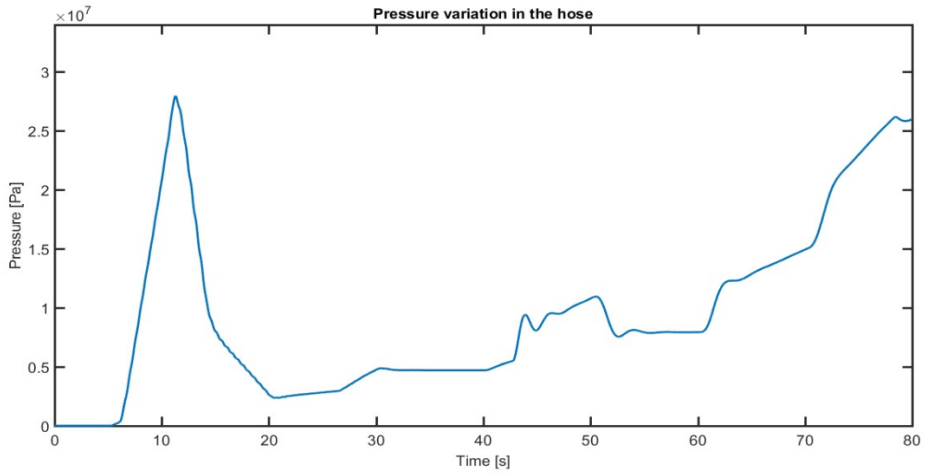

Figure 44. *Pressure fluctuation*

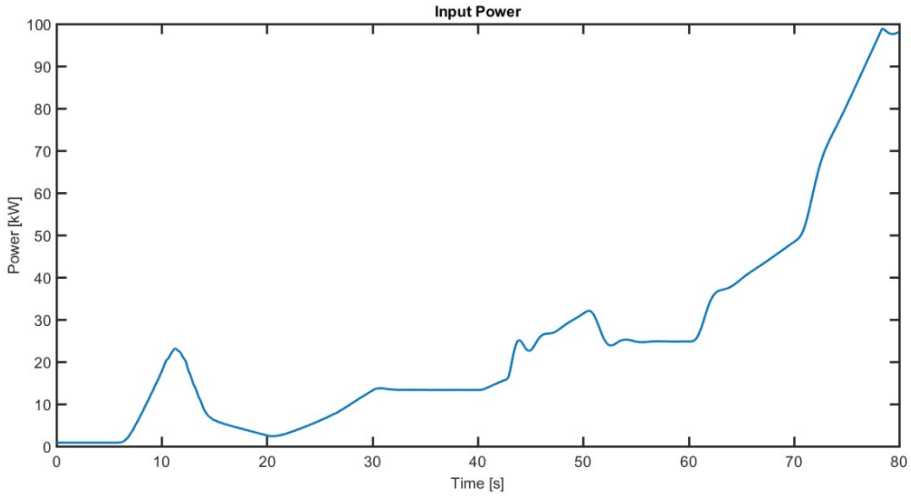

Figure 45. *Input (diesel engine) power*

In Figure 46, the fuel consumption of diesel engine for velocity in range of 0 – 27 km/h is demonstrated. Although increasing the traction force causes descending trend (from 530 g/kWh to 320 g/kWh) in the first 10 seconds, dropping the traction force and low rotational speed (means low power) result growing the fuel consumption rate to 510 g/kWh between seconds 10 and 20 (Figure 20). After this period, the velocity increases and as it is expected the fuel consumption rate goes down considerably to 298, 245, and 229 g/kWh at seconds 40, 60, 80 respectively.

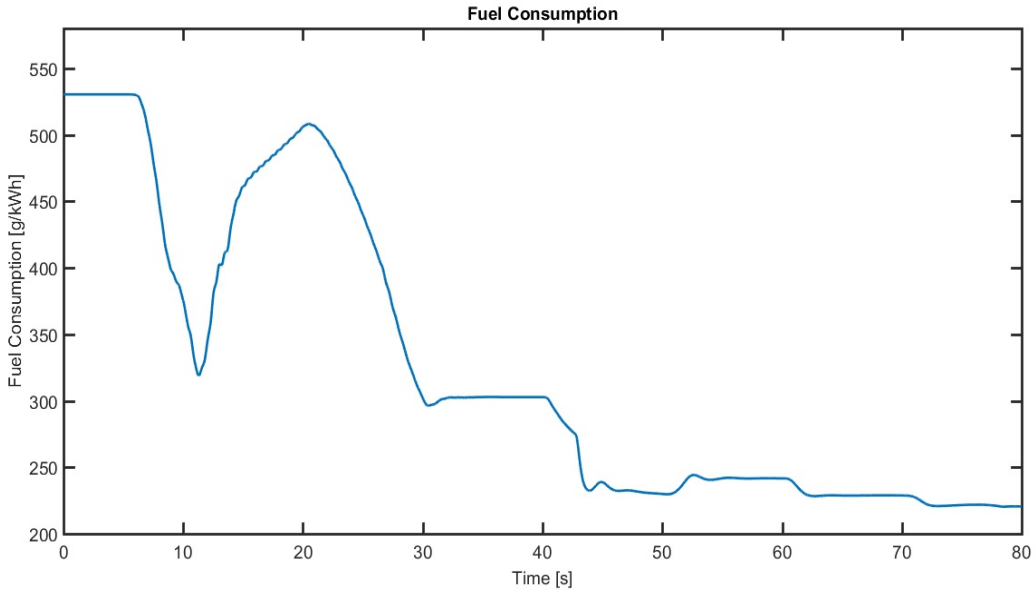

Figure 46. *Fuel consumption of diesel engine – velocity in range of 0-27 km/h*

Figure 47 shows the efficiency of the hydromechanical system. In this case, although it is above 85% in the first seconds, the both mechanical efficiencies of pump and motor effects adversely on total efficiency which is 70% in average and even reaches 68% between seconds 50 and 60.

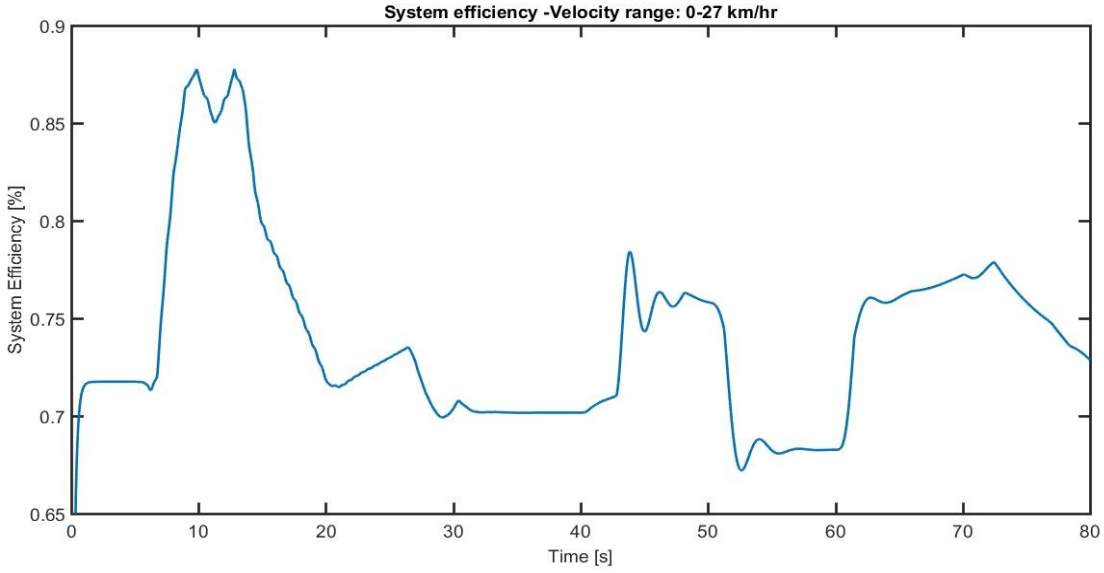

Figure 47. *The total efficiency of hydromechanical system*

3.2 PMSM simulation result

In chapter 2, the theory and model of PMSM were explained in detail, and the result of simulation will be evaluated in the below parts. Similar to the drive line simulation, the velocity trends are in the range of 0-8 km/h and 0-27 km/h. In the PMSM simulation, the velocity input should be in angular velocity (r/s) format. It means it should have the maximum velocity (km/h) resulted in angular velocity (r/s). The traction force is implemented as load torque in the simulation according to gear ratio.

3.2.1 Low speed range

In the velocity variation, the angular velocity varies 0 to 310 (r/s). in Figure 48, the result of simulation shows that the simulated speed could follow the reference rotational speed precisely. There are only some sensible oscillations at the high-speed level.

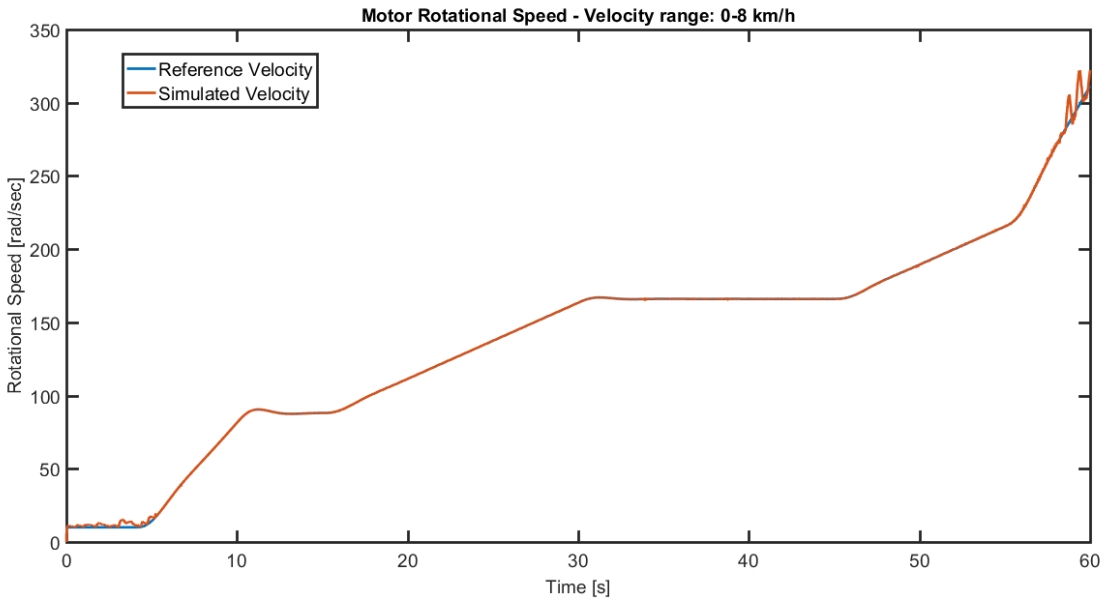

Figure 48. *The reference and measured (simulated) velocities trend*

Figure 49 demonstrates the load torque (due to traction force) and electromagnetic torque (produced by PMSM). The most prominent error is in the maximum traction force (maximum torque load) about 15% and then, the error between torques increased gradually from 6% to 100%. The reason is that according to equation 2-36, in the acceleration time, the system need more electromagnetic torque (load torque is constant), therefore, the difference between torques became significant.

In Figure 50, quadrature current variation is shown where its value increases by increasing the load (equation 2-35) and then, it has descending trend and apparently, the velocity increasing does not have the adverse impact on it.

In Figure 51, the direct current variation is illustrated which has been assumed to be zero. Although there are a lot of oscillations, their values are insignificant in comparison with quadrature current except the maximum velocity intervals where the current increased to 15 A.

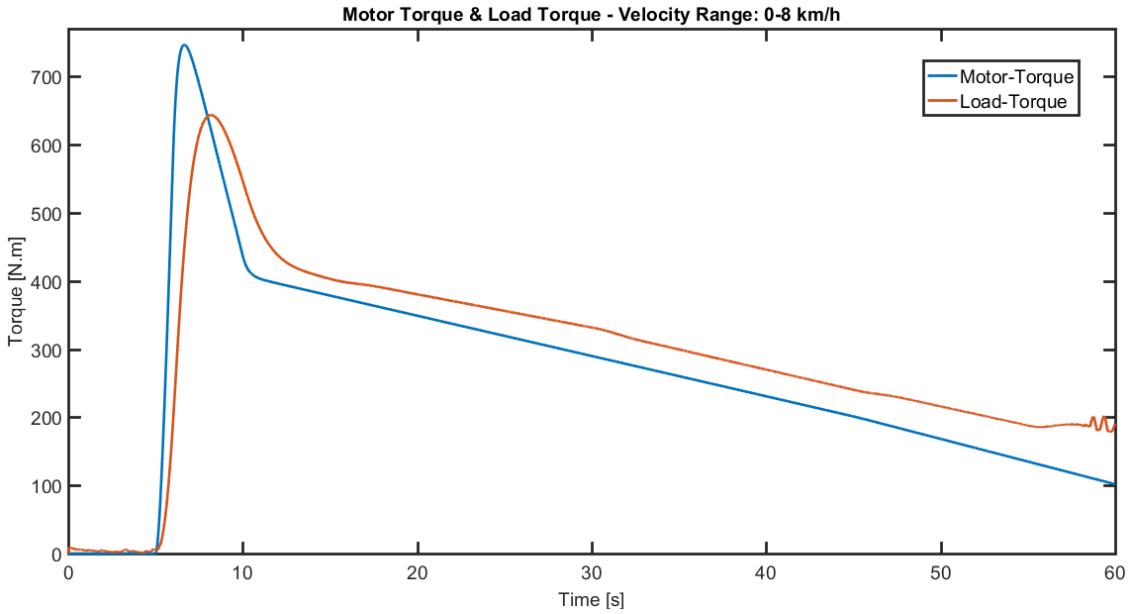

Figure 49. *The load torque (reference) and electromagnetic torque (simulated)*

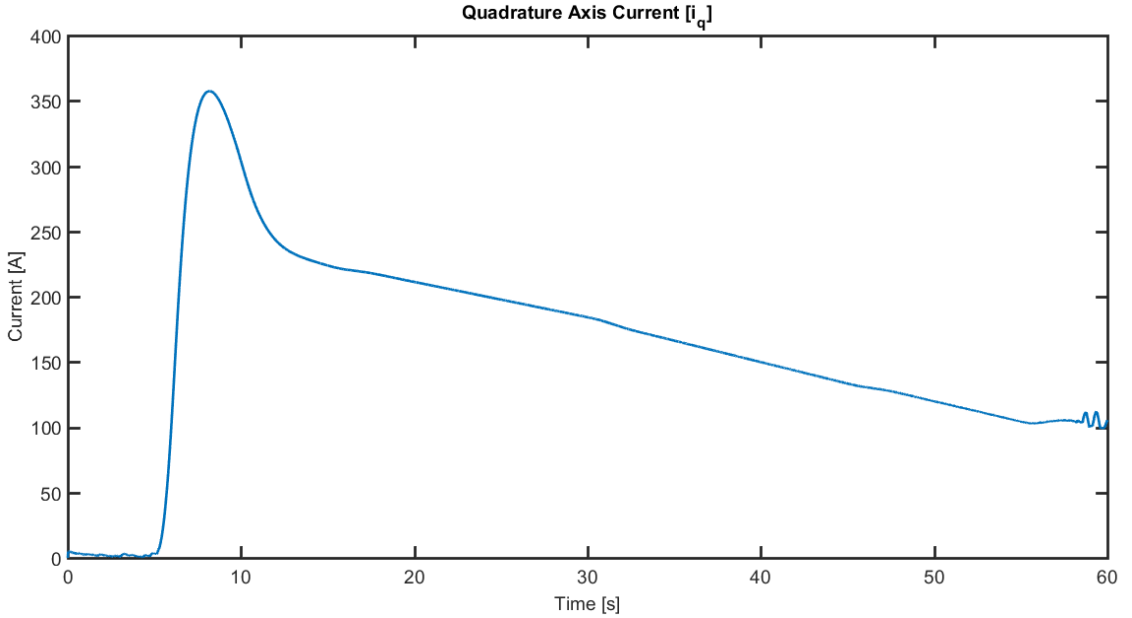

Figure 50. *The quadrature current*

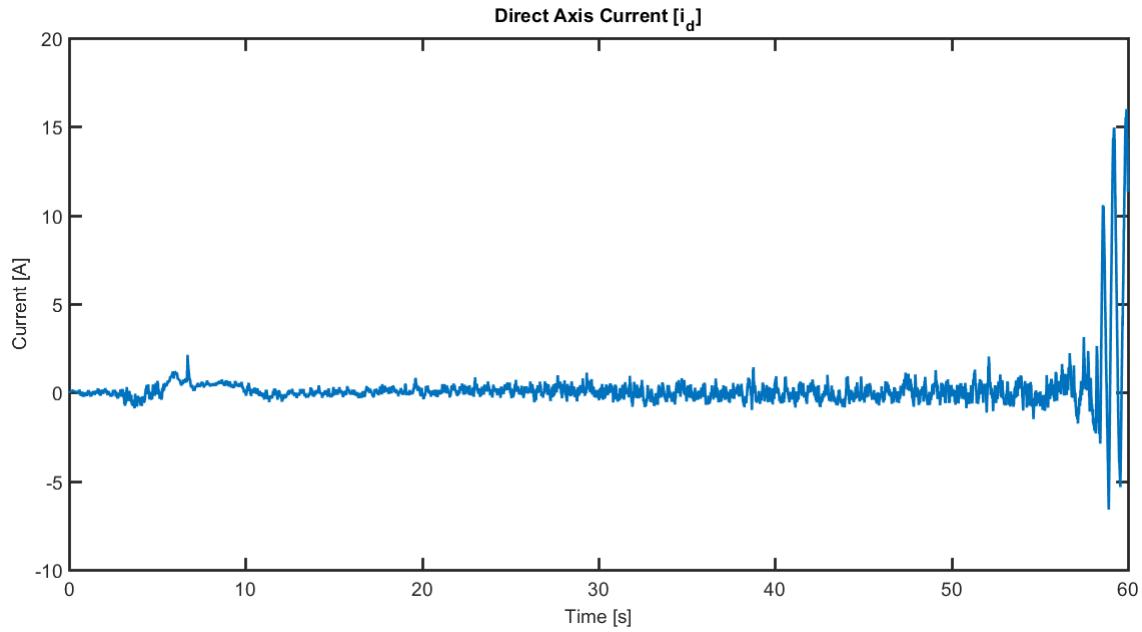

Figure 51. *The direct current*

The variation of PMSM voltage is shown in Figure 52. When the velocity starts ascending trend at second 5, the PMSM voltage goes up from 50 V to more 150 V. Then, the progressive trend of velocity leads to increasing the voltage to 400 V at the maximum speed.

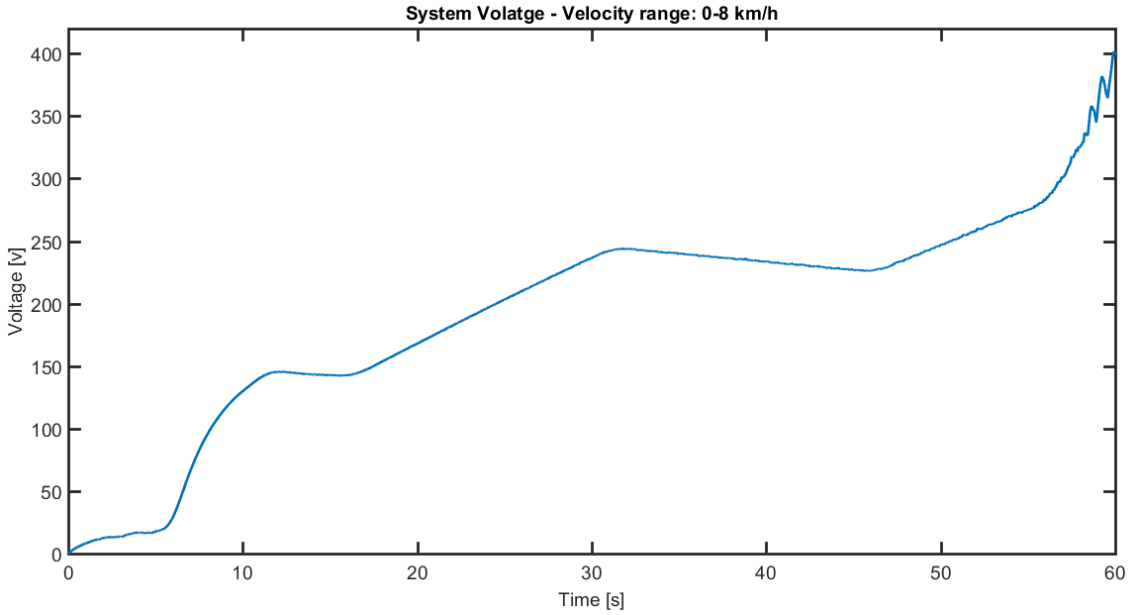

Figure 52. *The PMSM voltage*

The Figure 53 relates the efficiency of PMSM system. According to the electromagnetic torque and the rotational speed of PMSM, the efficiency has been mapped in where between seconds 0-5, the total efficiency is near 80%. Then, increasing the torque improves it to 86%. After dropping the efficiency due to the low electromagnetic torque, it has ascending trend t0 90% by raising the velocity. In time range 30-45 sec, the constant velocity and descending electromagnetic cause the efficiency decreases. As it was expected, the efficiency of PMSM is high, especially it is in range of 0.88-0.90 % in high velocity limit.

By comparing the Figure 53 with Figure 39, the higher efficiency of PMSM system can be observed easily. In Figure 39, after second 20, the efficiency goes down dramatically from 85% to 75% while the PMSM efficiency remains in range of 88 to 90%.

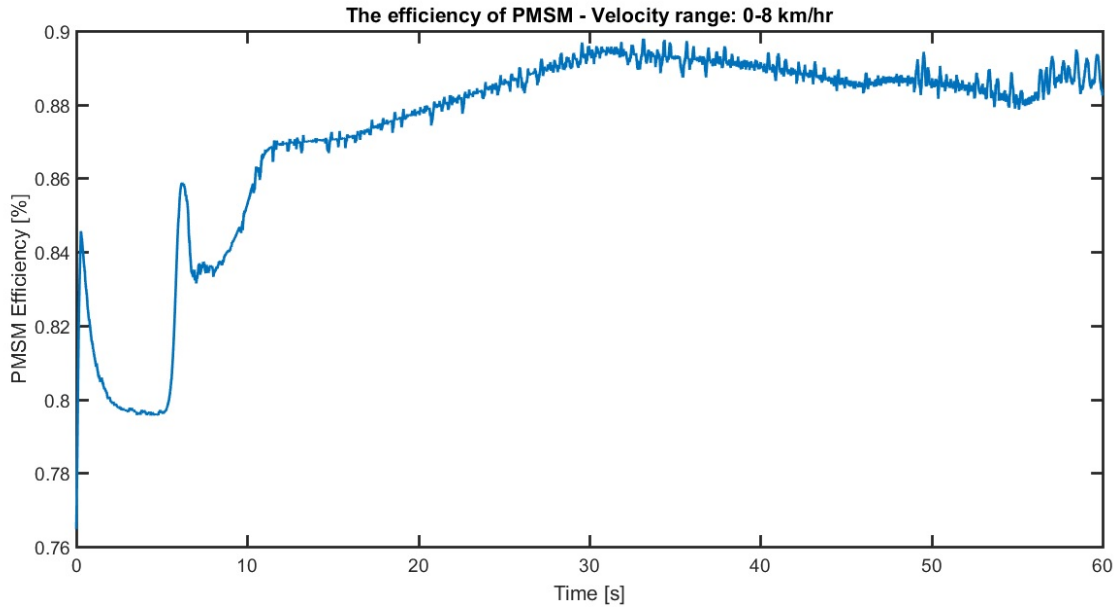

Figure 53. *The efficiency of PMSM*

3.2.2 High speed range

In the velocity trend, the angular velocity varies 0 to 405(r/s). The result of simulation, in Figure 54, shows that the difference between the reference and measured values is small except in the maximum velocity intervals which is around 6%. The main reason of considerable error in that the controller coefficients for both speed ranges are the same. Therefore, the simulated result cannot follow the reference values in the elevated level of machine velocity.

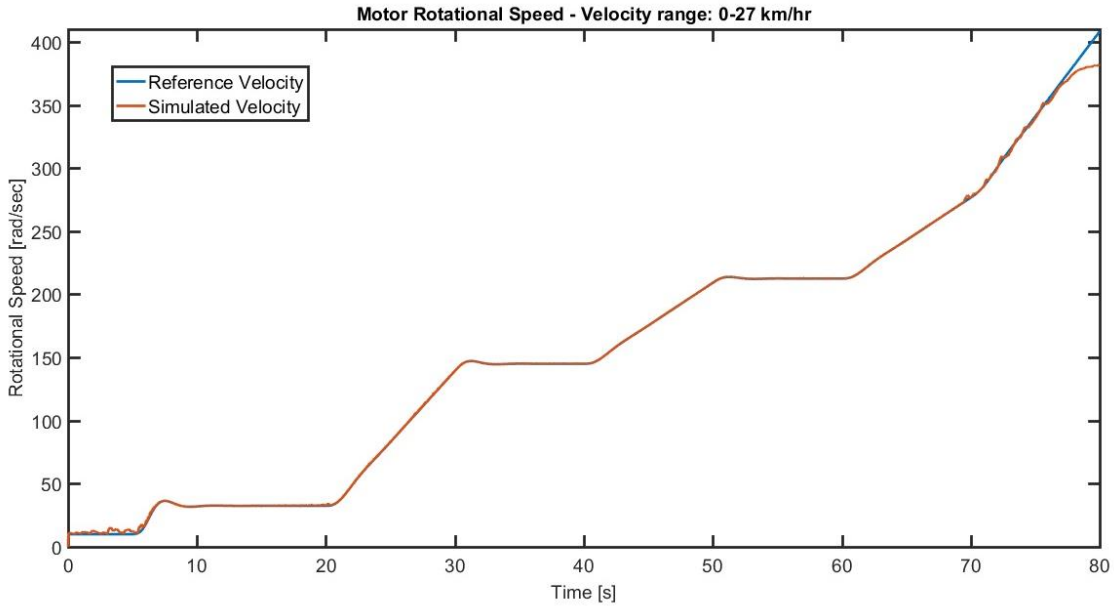

Figure 54. *The reference and measured (simulated) velocities trend*

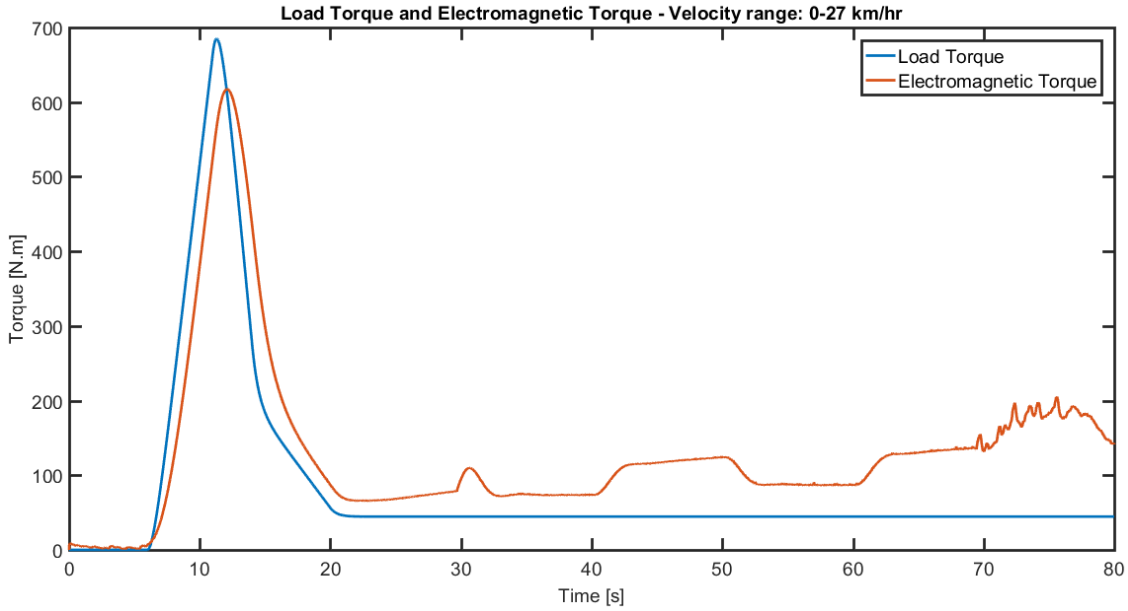

Figure 55. *The load torque (reference) and electromagnetic torque (simulated)*

Figure 55 demonstrates the load torque (due to traction force) and electromagnetic torque (produced by PMSM) during simulation time. The traction force and gear ration reduced three times simultaneously, consequently, the load torque did not change. But due to higher speed range, the electromagnetic torque had ascending trend from 80 N.m at second 20 to 200 N.m at second 76. Moreover, in the maximum load, the electromagnetic torque is around 600 N.m while in the low speed range, it was about 650 N.m. It means that in the high-speed range, the maximum current is lower than previous one.

As it shown in Figure 56, the maximum quadrature current is lower than the previous speed range (350 A Vs 480 A) because the maximum electromagnetic torque is 50 N.m lower than before. When the velocity has the ascending trend, the electromagnetic toque also goes up and clearly, it effects of the quadrature currents trend which increased from 48 A to 120 A approximately.

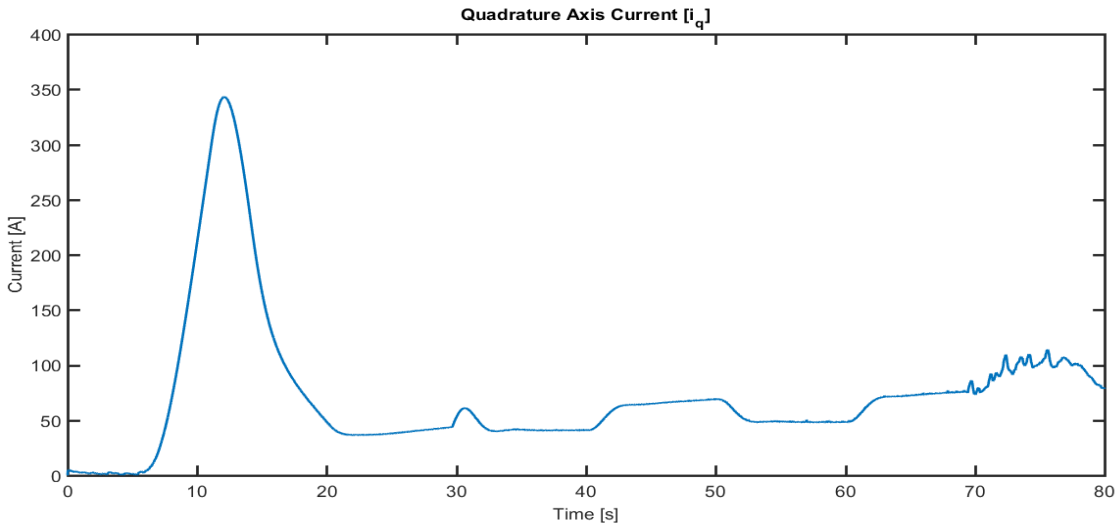

Figure 56. *The quadrature current*

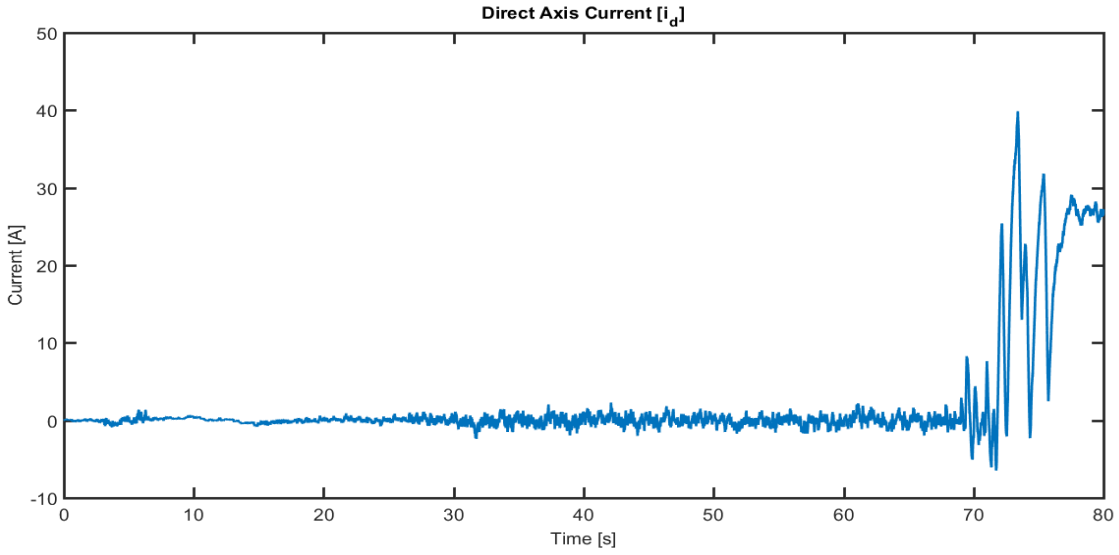

Figure 57. *The direct current*

In Figure 57, the direct current variation is shown which has been assumed zero. By comparing Figures 48,51,54,57, It can be recognized that the error in direct current has the same pattern as velocities error. When the simulated velocity can follow the reference velocity, the direct current error in tiny but when the velocity error goes up, the direct current goes up similarly though its value is ignorable by comparison with quadrature current.

Finally, the variation of voltage is demonstrated in Figure 58. In the maximum load torque, the voltage reached 70 V and next, it gained the 530 V when velocity went up to around 27 km/h. It worth to mention that significant oscillation between second 72 and 78 is because of currents variations.

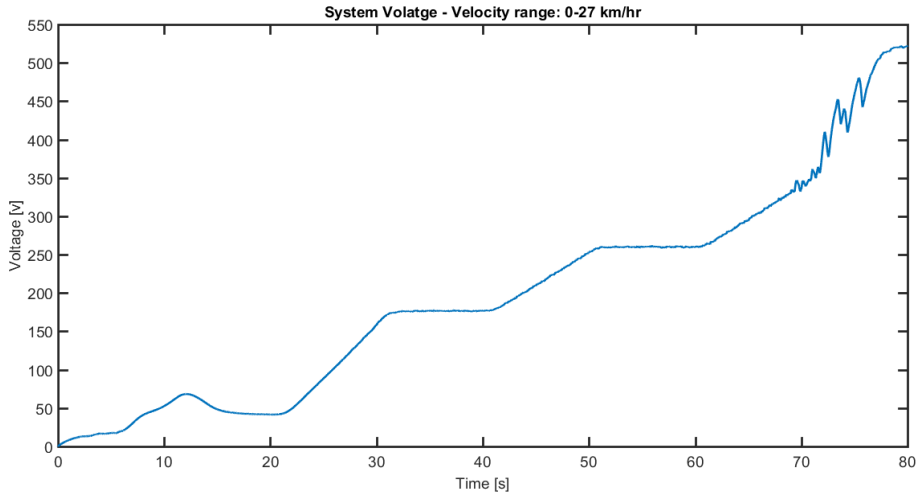

Figure 58. *The PMSM voltage*

In Figure 59, the fluctuation of PMSM efficiency is demonstrated. At the first moments, the efficiency is around 80% and then by increasing the velocity, the efficiency value increased gradually to reach 87%.

By comparing the Figure 59 with Figure 47, the higher efficiency in PMSM system can be observed easily. In Figure 47, after second 20, the efficiency is around 70% in average and even between seconds 50 and 60 is near 65% while in PMSM system, not only it is never lower than 80%, but also it raises to 87% after second 70. In simple words, the average of efficiency is 13 % bigger than the hydromechanical efficiency.

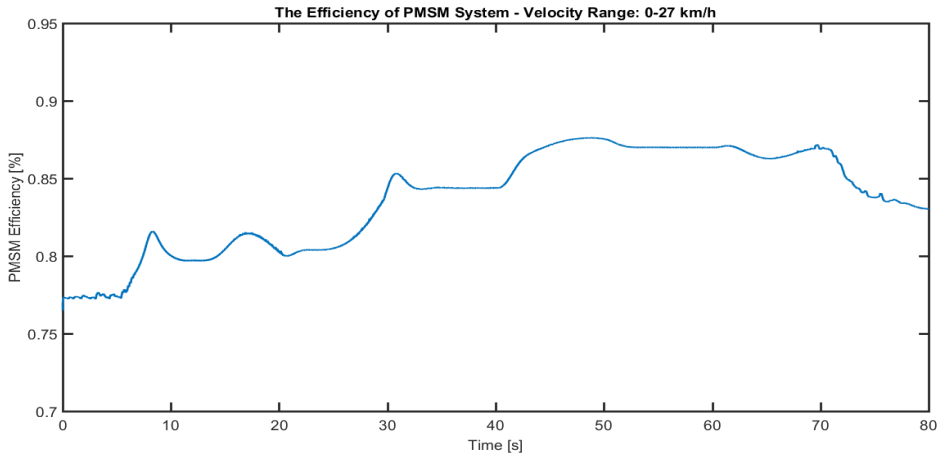

Figure 59. *The efficiency of PMSM*

4. DISCUSSION AND CONCLUSION

4.1 Conclusions

The aim of this thesis was modeling of one mobile hydraulic machine, ***Ponsse CARIBOU S10,*** in Simulink environment. In the first part, the drive line was modeled, and its operation was investigated in two different velocity ranges: 0-8 km/h and 0-27km/h. The errors between the reference/measured traction force and velocity were evaluated.

In the low speed range, the traction force error was between 8% and 15%. The measured velocity could follow the reference correctly in the beginning of simulation and then, the error increased gradually to 5%. Other important parameters of hydraulic system were evaluated such as pressure fluctuation and consumed power. Furthermore, the fuel consumption rate which had been mapped, was approximately 250 g/kWh around second 8. While the velocity increases, the power goes up (lower fuel consumption rate) and vice versa. Between second 15 and 30, the velocity range is 2-4 km/h. As a result, the fuel consumption rate goes down from 233 g/kWh to 218 g/kWh.

In the high-speed range, the error between the reference and measured traction force was insignificant in most of the simulation time due to its less value in comparison with previous condition; therefore, the controlling system could reduce the oscillation. Just at last moments of simulation, the difference went up around (15%), though it value is not considerable as much as the maximum traction force.

Assessment of velocity variation proved that although the controller led the measured velocity to have the same tendency of reference velocity, the error decreased from 20% to 10% approximately. As it was mentioned in previous chapter, the main reason of issue is that the controller parameters are the same for both velocity ranges. Like the first range, the prominent features of the system were illustrated such as pressure fluctuation and consumed power.

Indeed, the fuel consumption was mapped repeatedly where the velocity values achieved 8, 12, and 25 km/h, the fuel consumption rate declined to 298, 245, and 229 g/kWh. The maximum consumption rate gained only 229 g/kWh in the maximum velocity (27 km/h) (compare with the previous speed range, it achieved 218 g/kWh at 8 km/h)

In the second section, the hydrostatic power train was replaced with PMSM. The reference parameters were load torque (effect of traction force) and angular velocity (instead of linear velocity) in two velocity ranges: 0-8 km/h and 0-27 km/h. Other major features of the PMSM also investigated such as currents and voltage.

In the low speed range, the simulated velocity could follow the reference velocity precisely that the highest error was only 6%. In load and electromagnetic torque comparing, the maximum difference was 15% in starting seconds and then, it reduced to 6%.

In the high-speed range, the velocity could follow the reference value accurately near the maximum speed where the error raised to 9%. The issue of load torque (traction force) was similar completely to the former section. The maximum torque could be followed perfectly (4% variation) due to less value than the first condition but next, the error was rather noticeable (15%). Of course, the value of torque in tiny, itself, front of the maximum torque.

The primary objective of this research was assigned comparing the performance of hydromechanical system and PMSM system. The reference parameters were equal, so calculating the efficiencies can give extensive view about the operations of these systems. In the paragraphs below, it will be discussed in detail.

Canvassing the Figures 39 and 53 shows the performances of two systems with the same inputs (velocity range: 0-8 km/h). The PMSM performance is better that the hydromechanical system. By increasing the velocity, its PMSM efficiency fluctuation is between 87% and 89% while the hydromechanical efficiency goes down from 85% to 75%.

Similarly, the difference between Figures 47 and 59 proves the better performance of PMSM system. While the efficiency of hydromechanical system is around 73% during simulation time and even reaches the 65%, the efficiency of PMSM never be less than 80% and it keeps its ascending trend corresponding to velocity trend to gain 88%.

4.2 Future work

As it was mentioned several times, using the same controller for all conditions leads to considerable error for velocity or torque in the hydromechanical simulation. Therefore, designing various control systems for different operating conditions can be a good option, though the possibility of its implementation in the real system, robustness and smooth behavior should be evaluated in detail. Although modeling of diesel engine system which includes more parameters means more complexity in numerical process and necessity of a vast number of inputs, it can give great opportunity to analyze more accurate, behaved closer to the reality.

Apparently, there are several modeling methods for PMSM system with the variety of control approaches. For instance, surface -mounted magnets can be replaced with internal-mounted magnets (with saliency, IM) which occurs in the real machine or the battery simulation can be included in the model. Furthermore, it is suggested to use different controller (with different coefficients) for individual operating conditions.

To increase the precision of control system, the number of parameters, included in the controller should be more. Hysteresis control, stationary-frame control, synchronous-frame control can be embraced to the controller in order to improve its performance and avoid the noises. Also, using developed filters can remove unwanted fluctuation. Furthermore, implementing other types of control approaches such as direct torque controller, position-sensorless controller, current controller can be attractive topics for subsequent researches.

REFERENCES

1. F. Hosseinpour, H. Hajihosseini, “Importance of Simulation in Manufacturing”, World Academy of Science, Engineering and Technology, 27 2009.

2. V.R Stefanovic, “Trends in AC drive application”, Rockwell Automation, Standards Drives Division,1999.

3. Stadler E., Schiess I., 2000. Leistungssteigerung am Traktormotor, FAT-Berichte Nr. 555, Eidgenössische Forschungsanstalt für Agrarwirtschaft und Landtechnik, Switzerland

4. Merzoug and Benalla, “Nonlinear Backstopping Control of Permanent Magnet Synchronous Motor (PMSM)”, Department of Electrical Engineering, University of Mentouri Constantine. Algier 2010.

5. S. Chi “Position – sensor less control of permanent magnet synchronous machines over wide speed range”. Thesis for the degree of Doctoral, Department of Electrical and Computer Engineering, Ohio State University

6. D.V Munoz, “Design, simulation and implementation of a PMSM drive system”, Thesis for the degree of Master of Science in engineering, Department of Energy and Environment, Chalmers University of Technology, Gothenburg, Sweden, 2011.

7. F. Heydari, A. Sheikholeslami, K.G. Firouzjah, S. Lesan. “Predictive Field – Oriented Control of PMSM with space vector modulation technique”. Front, Electric, Electron, Eng. China. 2010.

8. S. Haghbin, “An Isolated Integrated Charger for Electric or Plug-in Hybrid Vehicles” thesis for the degree of licentiate of engineering. Chalmers University of Technology, department of Energy and Environment, Division of Electric Power Engineering. Gothenburg, Sweden, 2011.

9. P. Immonen, “Energy efficiency of a diesel electric mobile working machine”. Thesis for the degree of Doctor of Science (Technology) to be presented with due permission for public examination and criticism in the Auditorium 1382 at Lappeenranta University of Technology, Lappeenranta, Finland

‘Appendix A: Ponsse CARIBOU S10 Parameters

Own weight: 11950 Kg

Load: 10000 Kg ⟶ Total: 21950 Kg

Diesel engine: 91 kW/ 2200 RPM, 430 Nm/1450 RPM

Maximum traction force: 130 kN

Maximum speed: 1st gear ratio 0-8 km/h, 2nd gear ratio 0-27 km/h

Drive line: can use 100 % of the engine power when driving

Maximum pump displacement 90 cm3/rev

Maximum motor displacement 160 cm3/rev

Maximum Pressure 340 Bar

Articulated steering: Max angle 45 degrees, turning circle 6,5 m

Wheel: 4+4

Front 700/45-22.5, Rear 700/45-22.5

Front 600/50-22.5, Rear 600/50-22.5

Simulation Parameters:

```
% Hydraulic Motor:
motor.Vg = motor_Vg*1e-6*(3*tyyppi-2);   %[m^3/r] motor displacement
motor.tau = 0.2;                         %[-] time constant

% Hydraulic Pump:
pump.Vg = pump_Vg*1e-6;                  %[m^3/r] pump displacement
%[-] volumetrinenhyötysuhde
pump.tau = 0.2;                  %[-] time constant
pump.boost = p_boost*1e5;        %[Pa] boost pump pressure
pump.pSys = p_max*1e5;           %[Pa] pressure of system
pump.Vg_boost = boost_Vg*1e-6;   %[m^3/r] displacement of boost pump

% Hose
hose.Beff = hose_Beff;           %[Pa] Bulk module
hose.V = hose_V;                 %[m^3] volume of hose

% Load
cuorm.red_inertia1 = 0.8266; %[kgm2] load reduced inertia for all
cuorm.viscous_coef = 0.1743; %[Nms]load viscous coefficient
cuorm.d = 1.15;              %[m] the diameter
```

```
% Control
ctrl.t_init = 3; % [s] time after which the initial large viscose spin
will change to a lower count
init.p = 20e5;   % [Pa] system pressure at start
ctrl.v_gain = pi*rengas_d*(pump.Vg/motor.Vg)% is a coefficient of ro-
tation which is used to control the angle of the pump
```

Appendix B: Drive line calculation (Corner Power Theory)

a- The trend of velocity: 0-8 km/h

The power loss: 5% therefore 91-0.0.5*91=86.45 kW

$$R = \frac{F_D * V_D}{P_{max} * \eta_G * \eta_{tp} * \eta_{tm}} = \frac{130 * 10^3 * 8 * 10^3}{3600 * 86.45 * 10^3 * 0.98 * 0.93 * 0.9} = 4.07$$

Point 1:

$$Q_{p,1} = \frac{P_{max} * \eta_{tot,p}}{\Delta p_{max}} = \frac{86.45 * 10^3 * 0.93}{340 * 10^5} = 2.36 * 10^{-3}\ (\frac{m^3}{s})$$

$$V_{gp,1} = \frac{Q_{p,1}}{n_p * \eta_{v,p}} = \frac{2.36 * 10^{-3} * 60}{2200 * 0.97} = 6.64 * 10^{-5}\ (\frac{m^3}{r})$$

$$T_{m.1} = \frac{v_{gm,max} * \Delta p_{max} * \eta_{mh,m}}{2 * \pi} = \frac{160 * 10^{-6} * 340 * 10^5 * 0.95}{2 * \pi} = 822.5\ N.m$$

$$n_m = \frac{Q_{p,1} * \eta_{v,m}}{v_{g,m}} = \frac{2.36 * 10^{-3} * 0.95}{160 * 10^{-6}} = 14.01\ \left(\frac{rad}{s}\right)$$

$$F_1 = \frac{T_{m.1} * i_G * \eta_G}{r} = \frac{822.5 * i_G * 0.98}{0.575} = 130 * 10^3\ N\ \rightarrow i_G = 92.7$$

$$V_1 = \frac{2 * \pi * r * n_m}{i_G} = \frac{2 * \pi * 0.575 * 14.01}{92.7} = 0.55\ (\frac{m}{s})$$

Point 2:

$$Q_{p,2} = V_{g,pmax} * n_p * \eta_{v,p} = 90 * 10^{-6} * \left(\frac{22000}{60}\right) * 0.97 = 3.2 * 10^{-3}\ \left(\frac{m^3}{s}\right)$$

$$\Delta p_2 = \frac{P_{max} * \eta_{tp,2}}{Q_{p,2}} = \frac{86.45 * 10^3 * 0.93}{3.2 * 10^{-3}} = 251.24\ bar$$

$$n_{m.max} = \frac{8 * 1000 * 92.7}{3600 * 2 * \pi * 0.575} = 57\ \left(\frac{r}{s}\right)$$

$$v_{gm,min} = \frac{Q_{p,2} * \eta_{v,m}}{n_{m,max}} = \frac{3.2 * 10^{-3} * 0.95}{57} = 5.33 * 10^{-5}\ (\frac{m^3}{r})$$

$$T_{m,2} = \frac{v_{gm,min} * \Delta p_2 * \eta_{m,m}}{2 * \pi} = \frac{5.33 * 10^{-5} * 251.2 * 10^5 * 0.95}{2 * \pi} = 202.4\ N.m$$

$$F_2 = \frac{T_m * i_G * \eta_G}{r} = \frac{202.4 * 92.5 * 0.98}{0.575} = 31.9\ kN$$

$$V_2 = \frac{2 * \pi * 57 * 0.575}{92.5} = 2.22\ \left(\frac{m}{s}\right)$$

b- The trend of velocity: 0-27 km/h:

Due to increasing the velocity three times, therefore, the gear ration behalves three times approximately (i_G = 35)

$$R = \frac{F_D * V_D}{P_{max} * \eta_G * \eta_{tp} * \eta_{tm}} = \frac{130 * 10^3 * 27 * 10^3}{3600 * 86.45 * 10^3 * 0.98 * 0.93 * 0.9} = 13.8$$

Point 1:

$$Q_{p,1} = \frac{P_{max} * \eta_{tot,p}}{\Delta p_{max}} = \frac{86.45 * 10^3 * 0.93}{340 * 10^5} = 2.36 * 10^{-3}\ (\frac{m^3}{s})$$

$$V_{gp,1} = \frac{Q_{p,1}}{n_p * \eta_{v,p}} = \frac{2.36 * 10^{-3} * 60}{2200 * 0.97} = 6.64 * 10^{-5}\ \ (\frac{m^3}{r})$$

$$T_{m.1} = \frac{v_{gm,max} * \Delta p_{max} * \eta_{mh,m}}{2 * \pi} = \frac{160 * 10^{-6} * 340 * 10^5 * 0.95}{2 * \pi} = 822.5\ N.m$$

$$n_m = \frac{Q_{p,1} * \eta_{v,m}}{v_{g,m}} = \frac{2.36 * 10^{-3} * 0.95}{160 * 10^{-6}} = 14.01\ \left(\frac{rad}{s}\right)$$

$$F_1 = \frac{T_{m.1} * i_G * \eta_G}{r} = \frac{822.5 * 35 * 0.98}{0.575} = 49 * 10^3\ N$$

$$V_1 = \frac{2 * \pi * r * n_m}{i_G} = \frac{2 * \pi * 0.575 * 14.01}{35} = 1.45\ (\frac{m}{s})$$

Point 2:

$$Q_{p,2} = V_{g,pmax} * n_p * \eta_{v,p} = 90 * 10^{-6} * \left(\frac{22000}{60}\right) * 0.97 = 3.2 * 10^{-3}\ \left(\frac{m^3}{s}\right)$$

$$\Delta p_2 = \frac{P_{max} * \eta_{tp,2}}{Q_{p,2}} = \frac{86.45 * 10^3 * 0.93}{3.2 * 10^{-3}} = 251.24\ bar$$

$$n_{m.max} = \frac{8 * 1000 * 35}{3600 * 2 * \pi * 0.575} = 72.65\ \left(\frac{r}{s}\right)$$

$$v_{gm,min} = \frac{Q_{p,2} * \eta_{v,m}}{n_{m,max}} = \frac{3.2 * 10^{-3} * 0.95}{72.65} = 4.18 * 10^{-5} \left(\frac{m^3}{r}\right)$$

$$T_{m,2} = \frac{v_{gm,min} * \Delta p_2 * \eta_{m,m}}{2 * \pi} = \frac{4.18 * 10^{-5} * 251.2 * 10^5 * 0.95}{2 * \pi} = 158.6\ N.m$$

$$F_2 = \frac{T_m * i_G * \eta_G}{r} = \frac{158.8 * 35 * 0.98}{0.575} = 9.5\ kN$$

$$V_2 = \frac{2 * \pi * 72.65 * 0.575}{92.5} = 7.5\ \left(\frac{m}{s}\right)$$

Appendix C: PMSM parameters

```
% The PMSM parameters

Rs=0.012;            % Stator resistance
Lq=0.79e-3/sqrt(2); % Inductance (direct axis)
Ld=0.79e-3/sqrt(2); % Inductance (quadrature axis)
phi_pm=0.15;         % Flux linkage
p=6;                 % Number of poles
J=2.42;              % PMSM Inertia
Vdc=361;             % PMSM voltage
B=0.2;               % Viscous coefficient
Wbase=800*pi/30;     % Minimum rotational speed
Wmax=2800*pi/30;     % Maximum rotational speed
Prated=90000;        % Maximum PMSM power
Trated=860;          % Maximum PMSM torque
Fs=200e3;            % Switching frequency of inverter

%FOC coefficients

alpha_i=2*pi*Fs/10;
Kpc_d=alpha_i*Ld;
Kic_d=alpha_i*Rs;
Kpc_q=alpha_i*Lq;
Kic_q=alpha_i*Rs;

alpha_w=alpha_i/10;
Kpw=alpha_w*J;
Kiw=alpha_w*B;
```